N72-21829 N72-19847

NATIONAL AERONAUTICS AND SPACE ADMINISTRATION

## Technical Memorandum 33-528

## Solid-Propellant Motors for High-Incremental-Velocity Low-Acceleration Maneuvers in Space

John I. Shafer

CASE FILE COPY

JET PROPULSION LABORATORY

CALIFORNIA INSTITUTE OF TECHNOLOGY

PASADENA, CALIFORNIA

March 1, 1972

## Technical Memorandum 33-528

# Solid-Propellant Motors for High-Incremental-Velocity Low-Acceleration Maneuvers in Space

John I. Shafer

JET PROPULSION LABORATORY

CALIFORNIA INSTITUTE OF TECHNOLOGY

PASADENA, CALIFORNIA

March 1, 1972

## PREFACE

The work described in this report was performed by the Propulsion Division of the Jet Propulsion Laboratory.

#### NOTE

The International System of units is used throughout this report. The following conversion table can be used to obtain English unit equivalents:

To convert	to	divide by
centimeter	inch	2.54
centimeter <sup>3</sup>	inch <sup>3</sup>	$1.639\times10^{1}$
centimeter-newton	inch-pound	$1.130\times10^{1}$
meter	foot	$3.048 \times 10^{-1}$
kilogram	pound mass	$4.536 \times 10^{-1}$
newton	pound force	4.448
newton/centimeter <sup>2</sup>	pound/inch <sup>2</sup>	$6.895 \times 10^{-1}$
newton-second/kilogram	pound force-second/ pound mass	9.807

## CONTENTS

Absti	ract.	
I.	Intr	oduction 1
II.	Sys	tem Constraints 2
III.	Mot	or Design
	Α.	Physical Characteristics 5
	В.	Ballistic Factors
IV.	Con	nponent Development
	Α.	Charge Design and Propellant Development
	В.	Chamber Insulation
	C.	Low Acceleration-Rate Ignition
	D.	Nozzles for Long Burning Motors
V.	Den	nonstration Firings D-1 and D-1A
	Α.	Demonstration Firing D-1 79
	В.	Demonstration Firing D-1A
	C.	Comparisons of Short and Long Duration Motor Performance
VI.	Con	clusions
Refe	rence	es
TAB	LES	
]	Ι.	Pressure test results on case-bonded end-burning motors
II	Ι.	Characteristics of case-bonded end-burning motors for feasibility tests
II	ι.	Static firing feasibility tests of case-bonded end- burning motors
IV		Characteristics of case-bonded end-burning motors using Saturethane propellant

## CONTENTS (contd)

## TABLES (contd)

v.	Static firing results of case-bonded end-burning motors with Saturethane propellant	33
VI.	Characteristics of case-bonded end-burning motors using JPL 540 (trimodal) propellant	34
VII.	Characteristics of case-bonded end-burning motors using JPL 540 (trimodal) modified with Decanol	41
VIII.	Static firing results for case-bonded end-burning motors using JPL 540 (trimodal) modified with Decanol	42
IX.	Static-firing test conditions and results with all-carbon nozzles	72
x.	Characteristics of 355 kg demonstration motors	80
XI.	Static firing results for 355 kg demonstration motors	81
FIGURES		
1.	Jupiter Orbiter spacecraft	3
2.	Demonstration motor D-2	6
3.	Predicted ballistics for motor D-2	9
4.	Range of solid motor applicability	9
5.	Factors contributing to lower thrust motors	10
6.	Specific impulse efficiency versus pressure	12
7.	Characteristic length $L^*$ versus pressure at extinction	14
8.	Maximum acceleration and burning rate versus pressure	15
9.	Incremental velocity versus chamber pressure for different burning rates	17
10.	Motor curing and firing configurations	20
11.	Before and after slump of inverted motor at 79°C	25
12.	Buckled chamber after cooling from cure temperature	36

## CONTENTS (contd)

## FIGURES (contd)

13.	Tailoring propellant mechanical properties 38
14.	Propellant surface displacements in high L/D motor 44
15.	Slump motor propellant
16.	Launch simulation vibration tests on 355 kg slump motor
17.	Slump motor before axial vibration test 50
18.	Insulation erosion/char thickness versus exposure time
19.	The g-Dot ignition concept
20.	Mass flow rate ratio and chamber pressure versus burn time for main motor ignition delays of 0, 0.3, and 0.6 s
21.	Igniter mounted in motor
22.	The g-dot igniter
23.	g-dot igniter prototype and flame pattern
24.	Configuration of all-carbon nozzle for feasibility testing
25.	Layup step in nozzle transition and body fabrication 70
26.	All-carbon nozzle during simulated altitude firing
27.	All-carbon nozzle (a) before and (b) after simulated altitude firing
28.	Measured nozzle surface temperatures during and after static firing of flight-weight motor
29.	Predicted nozzle temperatures of 355 kg demonstration motor D-2
30.	Predicted and measured pressure-time program for motor D-1
31.	Predicted and measured pressure-time program for motor D-1A

## SOLID-PROPELLANT MOTORS FOR HIGH-INCREMENTAL-VELOCITY LOW-ACCELERATION MANEUVERS IN SPACE

John I. Shafer

Jet Propulsion Laboratory Pasadena, California, USA

#### ABSTRACT

Recent advancements in motor technology offer promise of extending the applicability of solid-propellant rockets into a regime of high-performance long-burning tasks beyond the capability of existing motors. Successful static test firings have demonstrated the feasibility of (1) utilizing fully case-bonded end-burning propellant charges without mechanical stress relief, (2) using an all-carbon radiative nozzle markedly lighter than the flight-weight ablative nozzle it replaces, and (3) producing low spacecraft acceleration rates during the thrust transient through a controlled-flow igniter that promotes operation below the L\* combustion limit. It remains now to show that a 350 kg-sized motor, with all features integrated, performs reliably and produces the predicted motor performance, a mass fraction of 0.92 with a vacuum specific impulse of 2840 N-s/kg.

#### I. INTRODUCTION

Development efforts on low-thrust, long-burning solid-propellant motor technology have been underway at JPL for approximately three years. Much

of the work is applicable for planetary atmospheric probes, inner-planet orbit-insertion motors and deorbit motors (Ref. 1). However, the efforts are oriented primarily toward orbit-insertion maneuvers at the planets Jupiter, Saturn, and perhaps Mercury, because of extensive scientific interest and recent NASA studies at JPL of outer planet orbiter missions. (Refs. 2 and 3.) Technology work was also initiated about a year ago with the Elkton Division of the Thiokol Chemical Corporation under a NASA contract. (Ref. 4.) It should be stressed that Jupiter, Saturn, and Mercury orbiter missions have not been authorized as flight projects as yet.

### II. SYSTEM CONSTRAINTS

An artists' rendering of a Jupiter orbiter spacecraft based on the TOPS concept is shown in Figure 1. It reveals some spacecraft system constraints on the propulsion subsystem. The two-year flight to Jupiter implies long vacuum storage for the orbit insertion motor before firing in the vacuum. The radiation from the radioisotope thermoelectric generator (RTG) power source implies long-term low-level gamma ray and neutron exposure. The latter especially is a new environment for solid-propellant motors. The envelope available for the motor, shown between the two large tanks of hydrazine, is quite restricted and favors a motor chamber length-to-diameter ratio, L/D, of about 1 to 2. The propulsion incremental velocity,  $\Delta v$ , required for orbit insertion is about 1500 m/s; since the motor constitutes 42% of the spacecraft mass, high motor-mass fraction and good specific impulse are mandatory.

Note the long, highly flexible appendages for the scientific instruments at the bottom and the RTG at the top. These dictate a spacecraft maximum acceleration tentatively set at 1 g until more detailed system analyses can be



Figure 1. Jupiter Orbiter spacecraft

made. The 1-g acceleration, in turn, implies inherently the low thrusts and long burning times of the current program. In addition, the very flexible appendages dictate low acceleration rates associated with starting thrust transients and again with motor thrust decay if limit-cycling of the guidance components is to be avoided, i.e., if the gyros are not to become saturated or go unstable.

Incidentally, thrust vector control, TVC, is not required from the solid-propellant motor during the orbit-insertion maneuver in this conceptual design. In the propulsion system under consideration, four 220-N throttleable hydrazine monopropellant engines provide the numerous stop-restart propulsive maneuvers such as midcourse correction, pre-encounter maneuvers near the planet, TVC during solid-propellant motor orbit-insertion, and finally orbit trim and perhaps a plane change in orbit. This is essentially the same concept as was utilized for the Surveyor Lunar Landing program.

Temperature limits for solid motor operation have been set at -18 to +43 °C. This is consistent with the temperature to be maintained within the propulsion compartment by active thermal control to avoid freezing the hydrazine (F. P.  $\cong$  1 °C).

#### III. MOTOR DESIGN

During the planetary studies it had been noted that JPL's radial-burning apogee motor for the Applications Technology Satellite (ATS) had most of the desired characteristics including successful operation in space. However, if applied as a scaled-up motor to deliver the required impulse, its spacecraft acceleration would be prohibitively high.

The design to be described resulted from adapting the ATS motor hardware, as a 73% by weight subscale motor, to the Jupiter orbiter mission requirements. In the broad technology effort that the adaptation necessitated, component concepts were to be tested in small 25-kg flight-weight motors salvaged from the successful Syncom program; these motors were subscale motors for the 345-kg ATS apogee motor. At approximately one-year intervals, the large modified ATS motor would be static fired to demonstrate those collective concepts found to be successful in the 25-kg motors as well as establish the progress of the program. Thus the first demonstration firing, D-0, established feasibility of the case-bonded end-burner at the large size, and demonstration firing D-2 should show in about 8 months that the 355-kg-sized motor, containing all the features required for a Jupiter orbiter mission, performs reliably and produces the predicted motor performance, a mass fraction of 0.92 with a vacuum specific impulse of 2840 Ns/kg.

#### A. Physical Characteristics

Motor D-2 is a subscale version about 90% of the diameter and length of the Jupiter orbiter motor in the recent JPL orbiter study. An artist's rendering of the 355-kg motor is shown in Figure 2.

The 71 by 71 cm motor chamber would use a titanium alloy machined to a wall thickness of 0.13 to 0.15 cm then chemically milled to 0.051 cm. The charge design is an end burner; it is unusual in that it is fully case-bonded and sealed to the chamber on all its lateral surfaces without mechanical stress relief. Burning takes place initially on both the conical and concave propellant surfaces, which recede to the right and left respectively (See Figure 2). The geometry was selected to produce a regressive thrust-time program and essentially a constant acceleration.

The propellant is an aluminized ammonium-perchlorate-polyether polyurethane system designated JPL 541. The oxidizer has a trimodal particle size distribution and is quite coarse in order to lower the burning

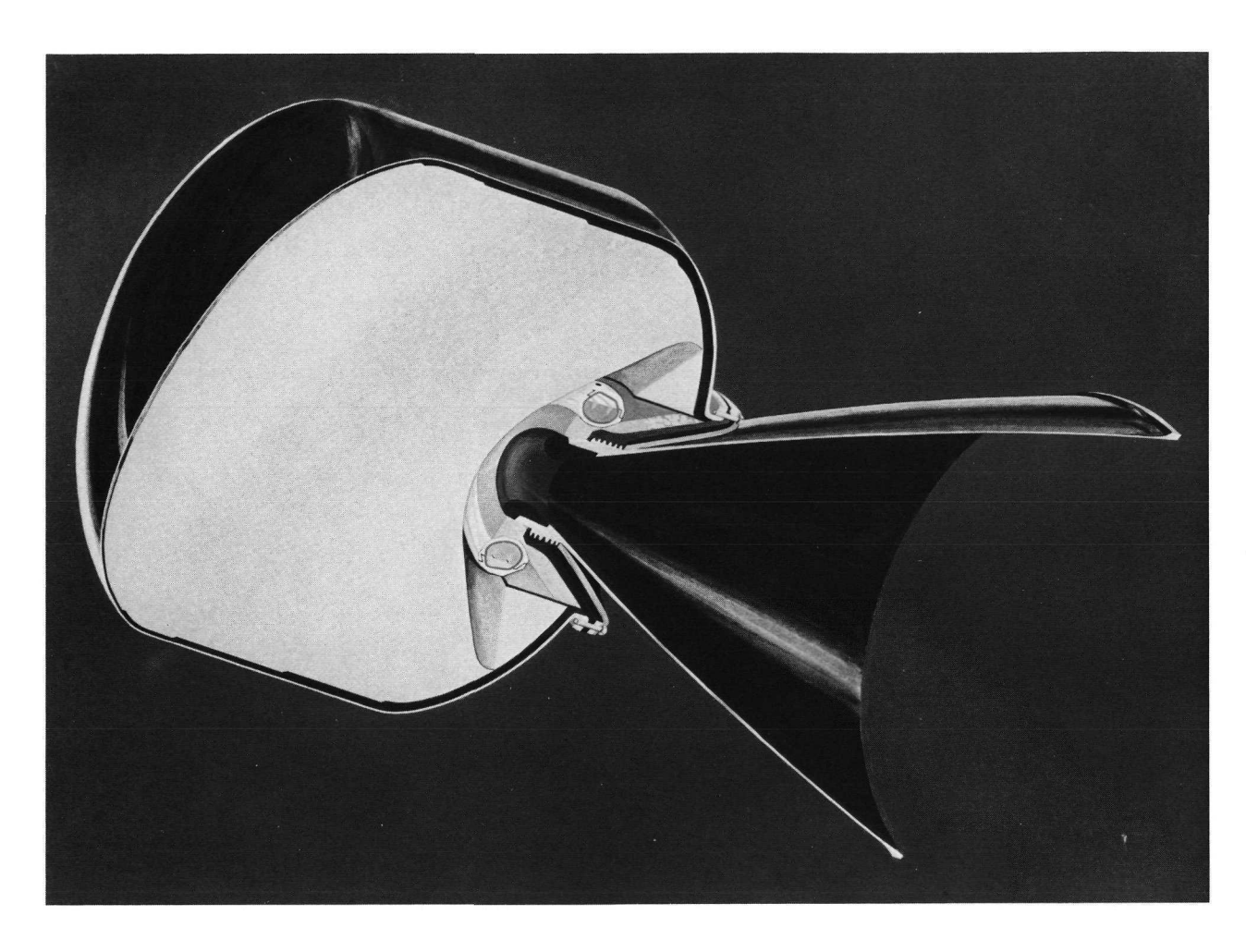


Figure 2. Demonstration motor D-2

rate. Mechanical properties have been tailored to give unusually high elongation to avoid propellant cracking or separation during motor cool down or chamber strain during firing; its initial modulus is very low to avoid buckling the thin-walled motor on cooling.

The chamber insulation is an asbestos/silica-filled ethylene propylene rubber that varies in thickness from 1 cm at the nozzle end to 0.2 cm at the forward end in accordance with its time of exposure to the flame. It serves the dual function of thermally insulating the chamber and inhibiting the propellant charge while bonding and sealing it to the former throughout all lateral surfaces except the burning faces.

The nozzle is a radiative type that utilizes a carbon composite (i.e., a carbon cloth in a carbon matrix) in the primary structure and expansion cone and operates with a cone surface temperature as high as 1660°C. It is one of the innovative design features of the motor and provides a significant extension in long burning-time nozzle capability.

The dish-shaped initial burning surface would have, for about 3 s, approximately 75% of its area inhibited (not shown). The torus-shaped igniter (called a g-Dot igniter at JPL) works in conjunction with the highly-inhibited initial burning surface to promote operation at pressures below its normal L\* combustion limit then building slowly to its maximum pressure. This ignition system provides the gentle 0.3 g/s acceleration rate needed by spacecraft components mounted on long flexible appendages. The low acceleration rate during thrust decay would be provided through the propellant charge geometry that is selected to produce automatically a gradual thrust tailoff.

The predicted weights for motor D-2 with its mass fraction of 0.92 are summarized as follows:

Component	Weight, kg
Chamber Insulation Nozzle Igniter Propellant	7.26 12.83 9.75 1.09 355.7
Motor total	386.6

#### B. Ballistic Factors

The calculated pressure, thrust, and acceleration programs are shown in Figure 3. The maximum acceleration, aided by the regressive thrust program, is only one g, well within the acceptable level. Of course if the D-2 motor were scaled up to Jupiter orbiter size by its linear factor of 1.1, the spacecraft maximum acceleration would only be 0.91 g.

- 1. Range of Solid Propellant Motor Applicability. When one compares, as a function of total impulse, the thrust-time requirements for this orbit-insertion class of motors with existing solid-propellant motors, it quickly becomes apparent that solid motor technology must be extended into a new regime beyond the present state-of-the-art (see Figure 4). The approximate range required for planetary orbiters is bounded by the box on the left and the approximate range of applicability of existing solid-propellant motors is indicated by the curved area. For a 1981 Jupiter orbiter with a 3/4-g acceleration limit, the motor must have a maximum thrust of about 8000 N and a burning time of about 194 s; today's long-duration motors at that thrust level have an order of magnitude shorter burning time, about 16 to 19 s. This explains then, why it is necessary to utilize all available approaches for adjusting the thrust program in order to meet the acceleration requirement.
- 2. Approaches to Lower Acceleration. The thrust-time programs of Figure 5 illustrate the influence of the factors utilized. If a reference radial-burning motor with a constant thrust program based on the 345-kg ATS were

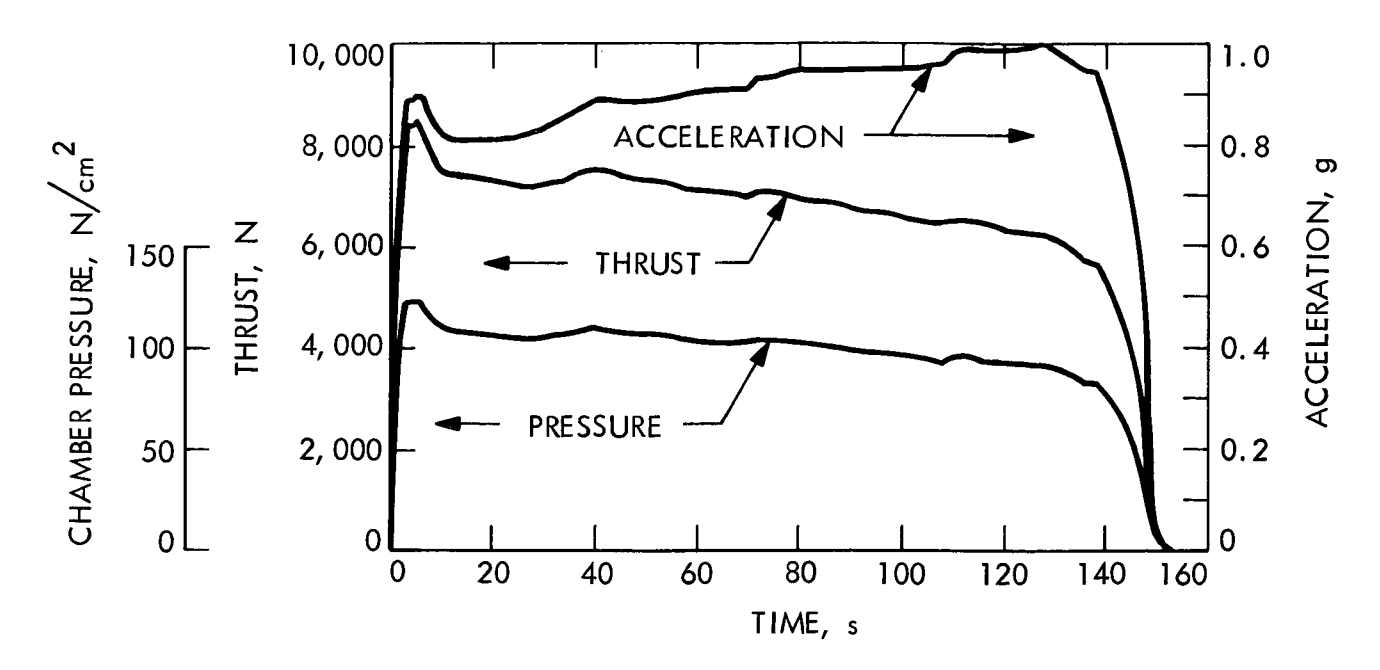


Figure 3. Predicted ballistics for motor D-2

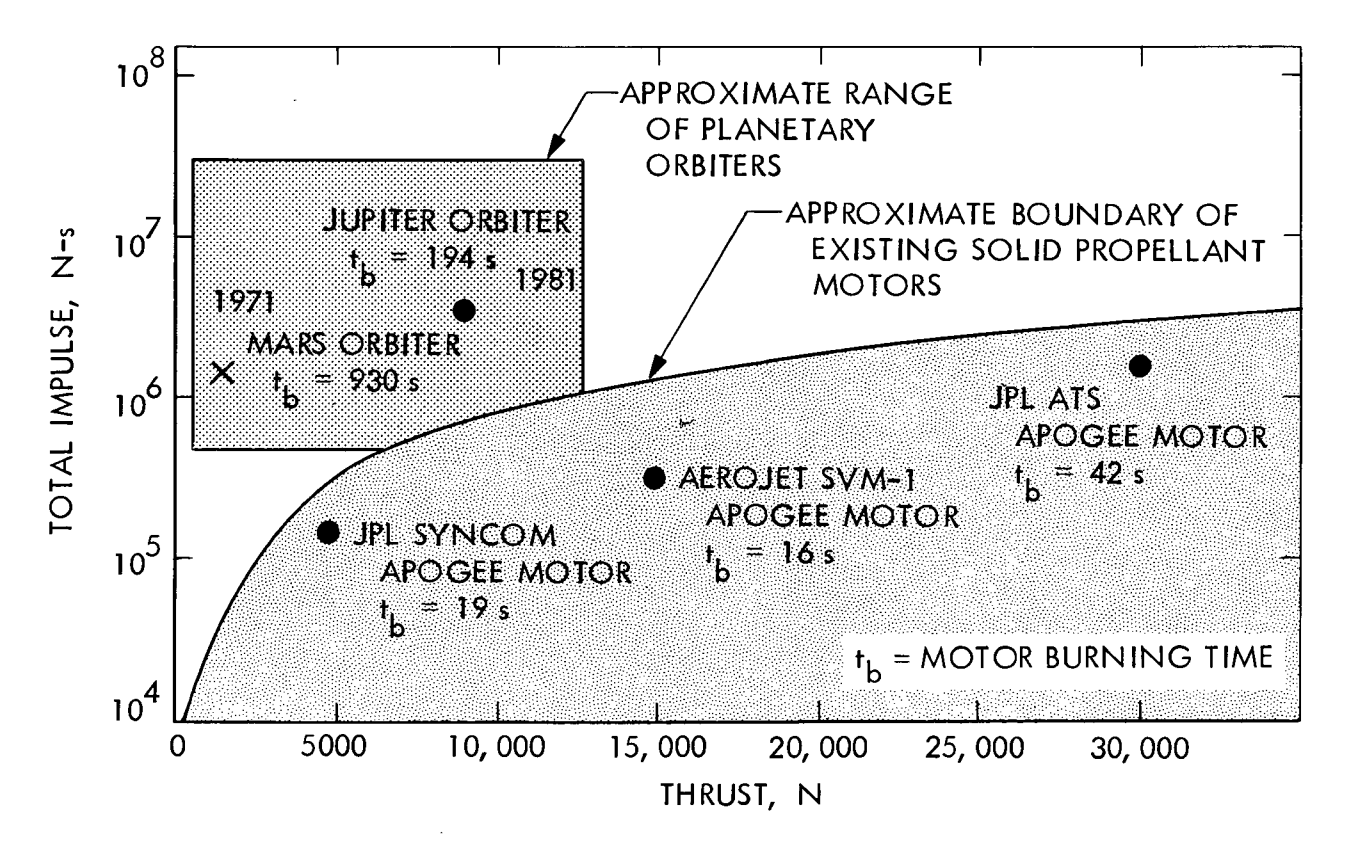


Figure 4. Range of solid motor applicability

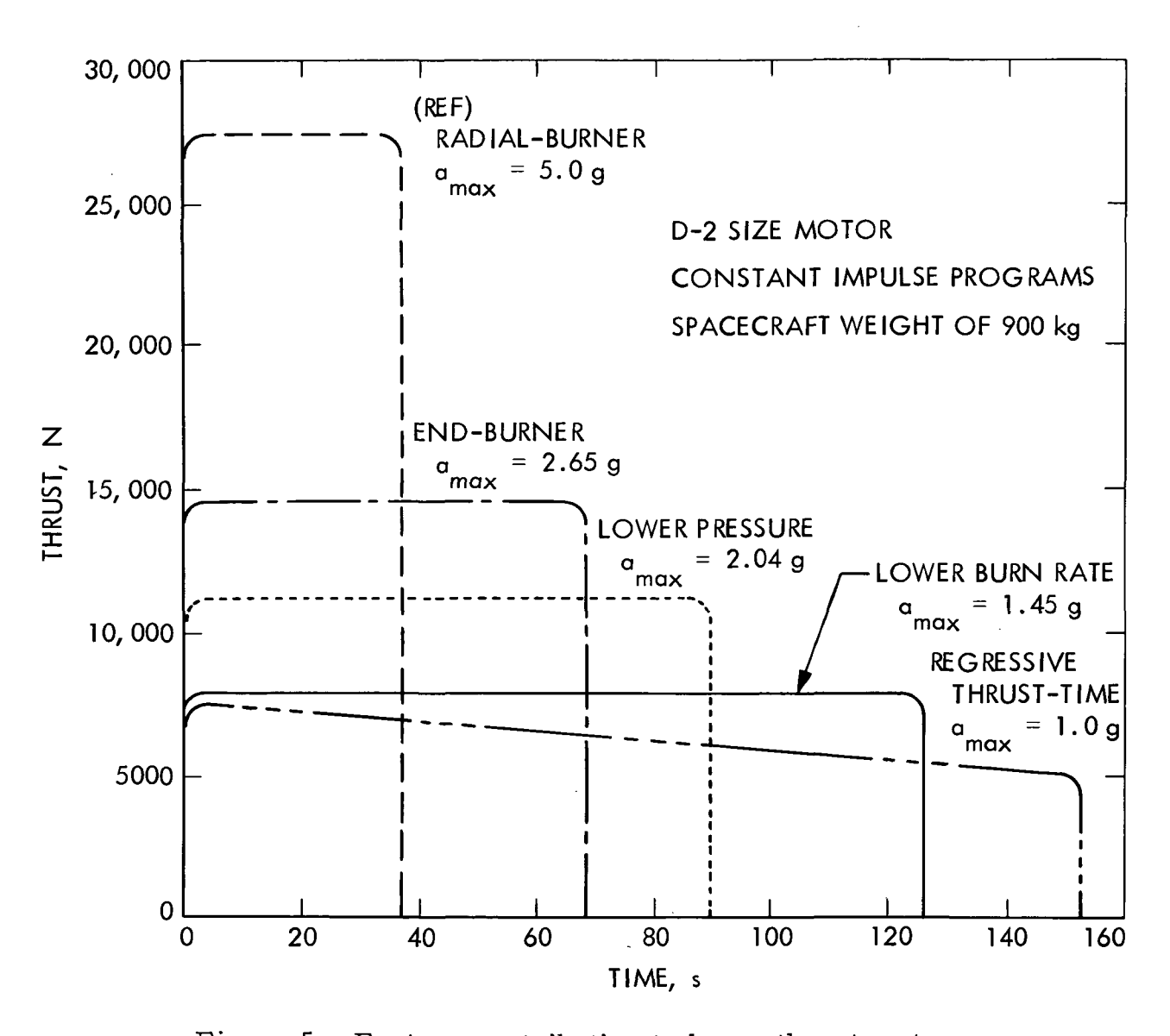


Figure 5. Factors contributing to lower thrust motors

used in the spacecraft being inserted into orbit, the maximum acceleration would be 5.0 g. By merely substituting an end-burner, the maximum acceleration would become 2.65 g. On lowering the mean pressure from the ATS's 143 N/cm<sup>2</sup> to 103 N/cm<sup>2</sup>, it decreases to 2.04 g (but at some risk of lower specific impulse efficiency and performance). By then decreasing the propellant burning rate 29% (at the given pressure) through the use of coarser oxidizer and oxamide\*, a burning rate depressant, it would become 1.45 g. Finally, by shaping the end-burner geometry to produce the regressive thrust-time program, the desired 1-g maximum (our interim goal for a D-2 sized motor) would be obtained. A corollary to the above can be made: radial-burning motors using propellants with the burning rates available today cannot meet the low-acceleration requirements of the planetary orbiter missions when the chamber L/D is one.

a. <u>Pressure</u>. Adoption of a lower chamber pressure would not only help reduce the thrust and spacecraft acceleration, as noted above, but should also reduce the erosion/char rate of the motor insulation (and nozzle if it is an ablative design), thus enhancing motor mass fraction and performance. However, pressures as low as 100 to 150 N/cm<sup>2</sup> have been avoided in the past in the rocket industry because of a concern that the propellant specific impulse efficiency for aluminized propellants would be substantially lower than at high pressures as is the case with berylliumized propellants.

Figure 6 shows specific impulse efficiencies from some JPL static test firings with aluminized and berylliumized propellants in ballistic evaluation (BATES) motors at the Arnold Engineering Development Center. Results from one Syncom firing and 8 ATS qualification firings at the same facility

<sup>\*</sup>H2NCOCONH2

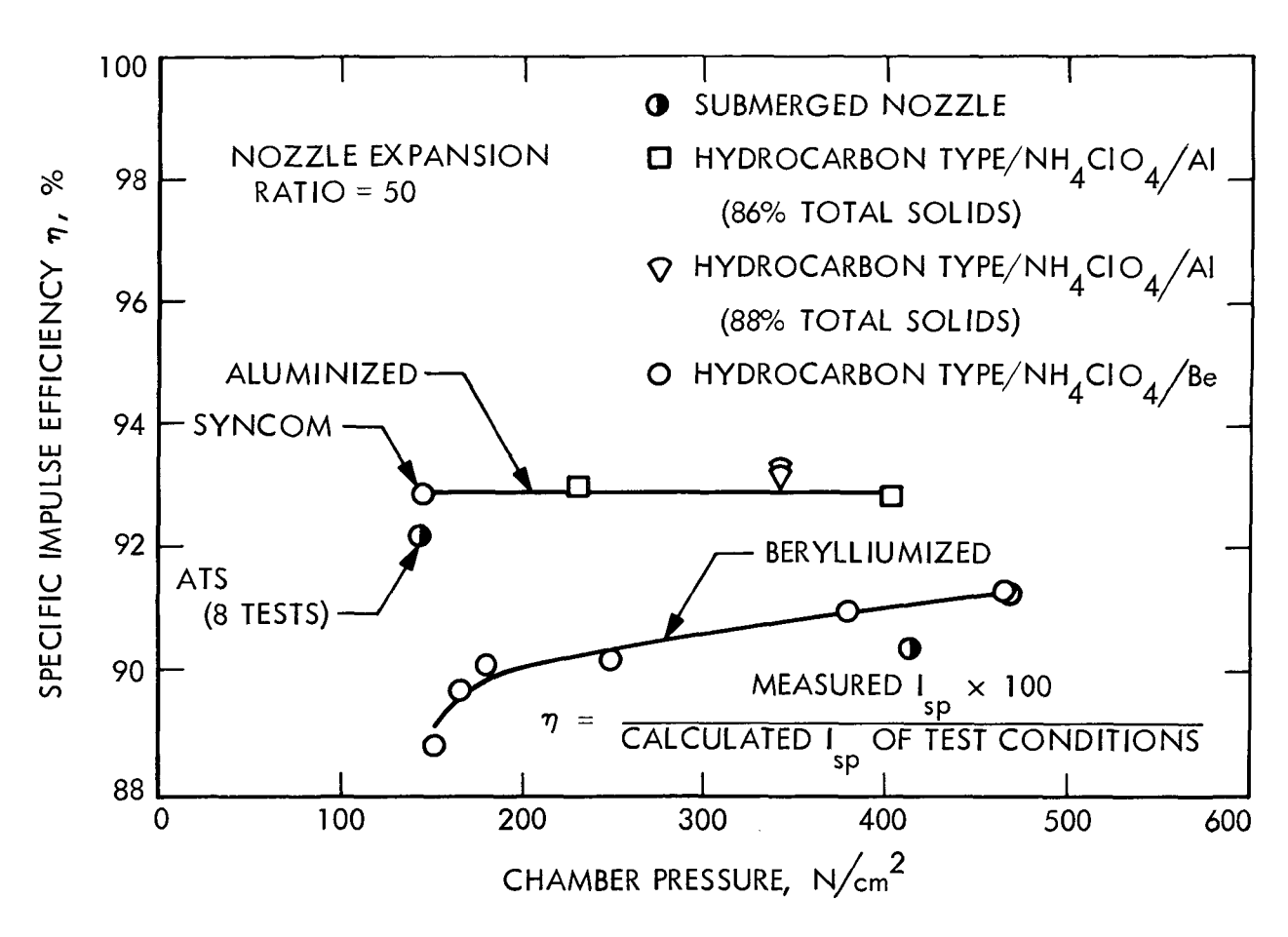


Figure 6. Specific impulse efficiency versus pressure

are included. All 8 tests of the ATS motor fell within  $\pm 0.1\%$  of the mean value. The 8 ATS motors and one motor with berylliumized propellant used submerged nozzles; the other motors used external nozzles. There is good evidence from other independent tests, as well as these, that specific impulse efficiencies for submerged nozzles turn out to be about 0.5 to 1.0% lower than for external nozzles. Thus, when all motor firings in Figure 6 are compared on the same basis, it is obvious that efficiency of the aluminized propellants is unimpaired at least down to pressures as low as  $143 \text{ N/cm}^2$ . Therefore, the decision to operate the new motor at pressures as low as 80 to  $100 \text{ N/cm}^2$  was considered an acceptable risk; indeed efficiencies at these pressures were deemed well worth checking.

On the other hand, operation at low initial chamber pressures, in combination with high propellant-volumetric loading, results in low L\* values (i.e., motor free volume to nozzle throat area ratio) and the possibilities of ignition difficulty and L\* instability. This was an important consideration in meeting the acceleration rate requirement and resulted in the g-Dot igniter concept. Figure 7 shows L\* versus chamber pressure for propellants JPL 540, JPL 540 (Trimodal) and JPL 541. The first of these propellants was on hand at the beginning of the program; the second was intended as an interim propellant of lower burning rate; finally, the JPL 541 formulation has an even lower burning rate, that desired for motor D-2. Extinction pressures for these propellants tend to be somewhat higher than, for example, propellants with hydrocarbon-type binders for a given L\*.

b. Effect of burning rate and pressure on acceleration and incremental velocity. The effect of propellant with different burning rates on the space-craft maximum acceleration for different chamber pressures is shown in Figure 8. Final pressure was selected, rather than maximum or mean

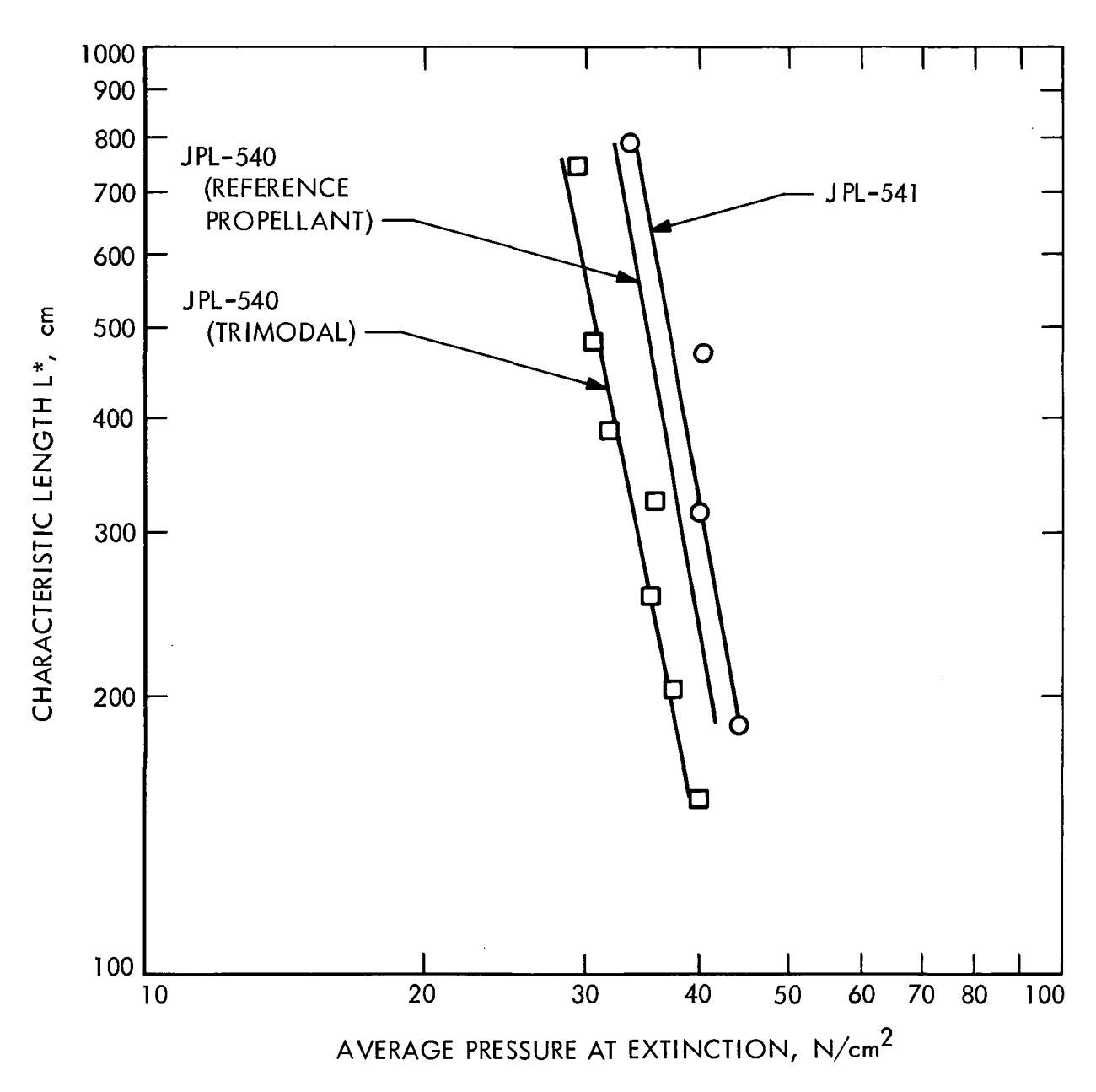


Figure 7. Characteristic length L\* versus pressure at extinction

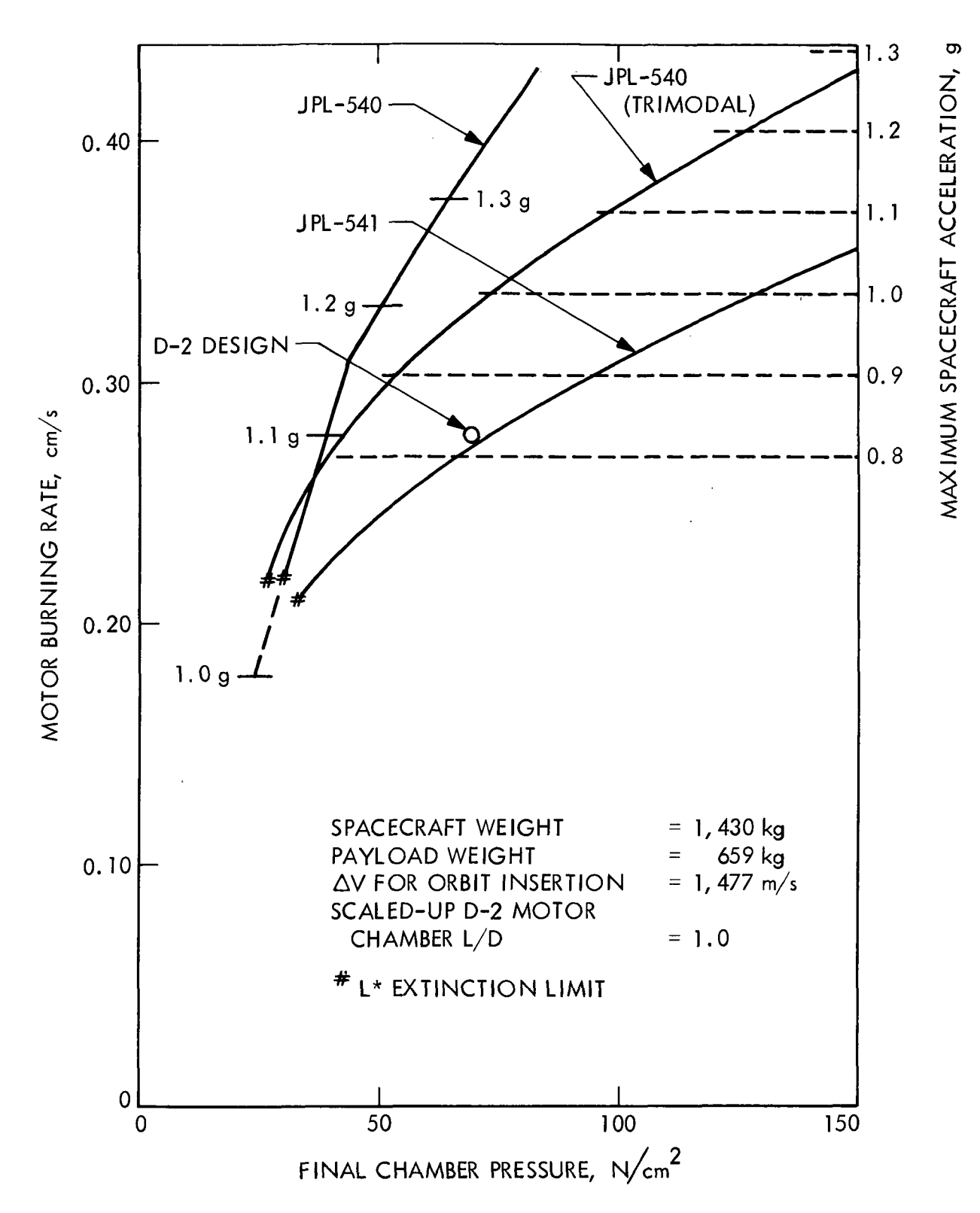


Figure 8. Maximum acceleration and burning rate versus pressure

effective pressure, because the critical parameter, maximum acceleration, is usually found at or near the end of firing.

Note in Figure 8 that propellant JPL 540, one of the lowest burning-rate, high-performance propellants available at the beginning of the program, would produce a spacecraft acceleration in excess of the 1-g level required; at 24 N/cm<sup>2</sup>, the final chamber pressure would be below the L\* combustion limit of 30 N/cm<sup>2</sup> and extinction would have occurred before the propellant had been consumed. JPL 540 has two changes in the slope of the burning rate curve; it was necessary therefore to show acceleration levels as tick marks on the curve itself.

JPL 540 (Trimodal), developed during the program, dropped the burning rate to the point where the interim acceleration goal was attained. Further reduction in burning rate gave a propellant (JPL 541) that established major progress in reaching the ultimate goal of about 0.75 g, or, alternately, allowed operation at higher chamber pressure if specific impulse efficiency proved to be unacceptable in static firings at low chamber pressure.

Figure 9 extends the study to show how the orbit insertion incremental velocity would be affected by motor chamber pressure for the same group of propellants. In the preceding Figure 8, low burning rate and low pressure are favored to obtain a low enough spacecraft acceleration; to obtain high incremental velocities as plotted in Figure 9, however, one favors high burning rates and low pressures. Obviously too, propellants with low L\* extinction pressures are favored if propellant I sp efficiency does not suffer with operation at low pressure (c.f. Figures 8 and 9).

The values and slopes of the curves in Figure 9 are rather sensitive to the relationship for insulation erosion/char thickness versus burning time; the plots are of greatest value in indicating approximations and trends. Even so, further development work is not expected to alter them drastically.

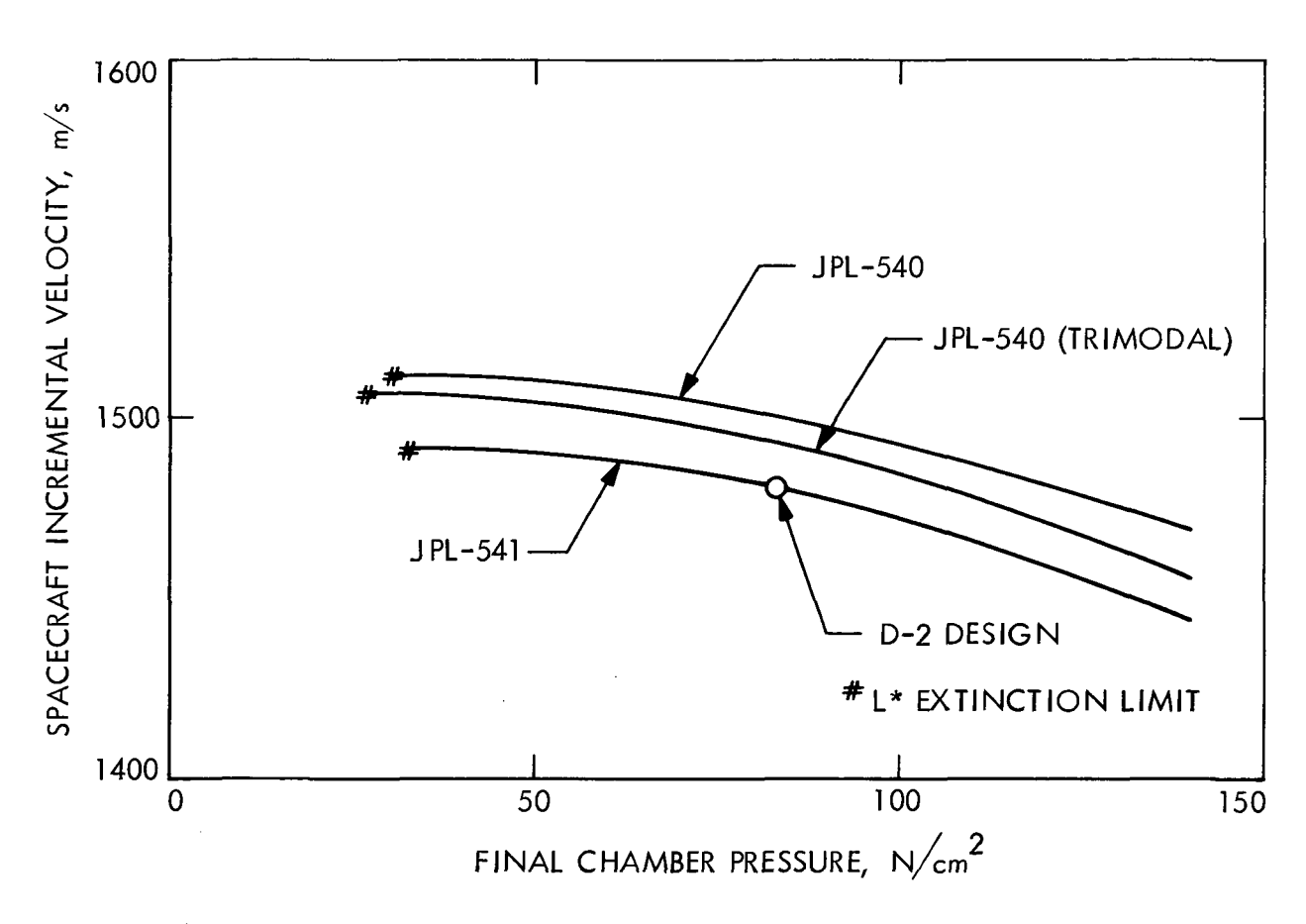


Figure 9. Incremental velocity versus chamber pressure for different burning rates

#### IV. COMPONENT DEVELOPMENT

Although this is a motor technology report, the development philosophy has been influenced strongly by the fact that the effort was projected-oriented. The motor has several unconventional features that could ultimately raise the question of "motor unreliability." Because reliability of the motor could not be established by statistical testing, the philosophy of evaluating critical design features with margins at limit loads was adopted at the beginning of the program, e.g., testing at 20 to 50% beyond the maximum expected pressure and chamber strain, vibration load, or operating temperature extremes. Also, nondestructive testing such as radiography and pressure testing prior to static firing was conducted to insure that detectable failures were not present. Such an approach coupled with a static test firing record that is 100% successful is a potent argument that reliability is indeed in hand despite the innovations.

However, such a success-oriented approach has the disadvantage of conservative implementation; thus, all factors that may contribute to success are usually adopted to help insure success. Today we find, if the mathematicians phrase may be twisted, that all of the processing steps for the casebonded end-burner and the design features for the all-carbon nozzle "are sufficient; they may not be necessary." Thus feasibility and proof of the concepts have been carried out as of this date. However, additional refinements are necessary to establish the optimum processing and component designs.

The philosophy, above, that advocates success in the demonstration (i.e., showcase) static test firings through conservatism does not imply that "failures" at earlier development stages of processing or testing are unacceptable—or even undesirable in some cases. "Failures" can be and

were invaluable in differentiating between the acceptable and unacceptable design or technique.

The experimental program and results are discussed below in essentially chronological order by component.

### A. Charge Design and Propellant Development

The greatest single change in realizing low acceleration came, as noted earlier, from the adoption of the end-burning design — in our efforts, a casebonded end-burner. Because the propellant properties and the end-burner are so closely interrelated and the work was conducted concurrently, the two will be discussed together. Indeed it was the availability of propellant, JPL 540, with its unusually high elongation at maximum stress, 80-100%, and low modulus, 120 to 70 N/cm<sup>2</sup>, that prompted consideration of a fully case-bonded motor.

It is believed that case-bonded, in contrast to cartridge and mechanically stress-relieved, end-burning motors will (1) provide a simpler design, (2) increase motor mass fraction by reducing insulation weight and increasing propellant weight and (3) maintain better support against charge creep in storage, ground handling forces, and vibration and inertial acceleration forces during vehicle launch.

Motor processing tests and static firings on the case-bonded end-burner were carried out with thin-walled flight hardware so that motor strains and stresses would be more realistic. A cross-section of the 25-kg motor is shown in Figure 10, the curing configuration on the left, the firing configuration on the right.

There was concern primarily about two types of failure modes:

(1) During cure at 60°C, solidification of the propellant occurs first all around the outside then gradually progresses inward toward

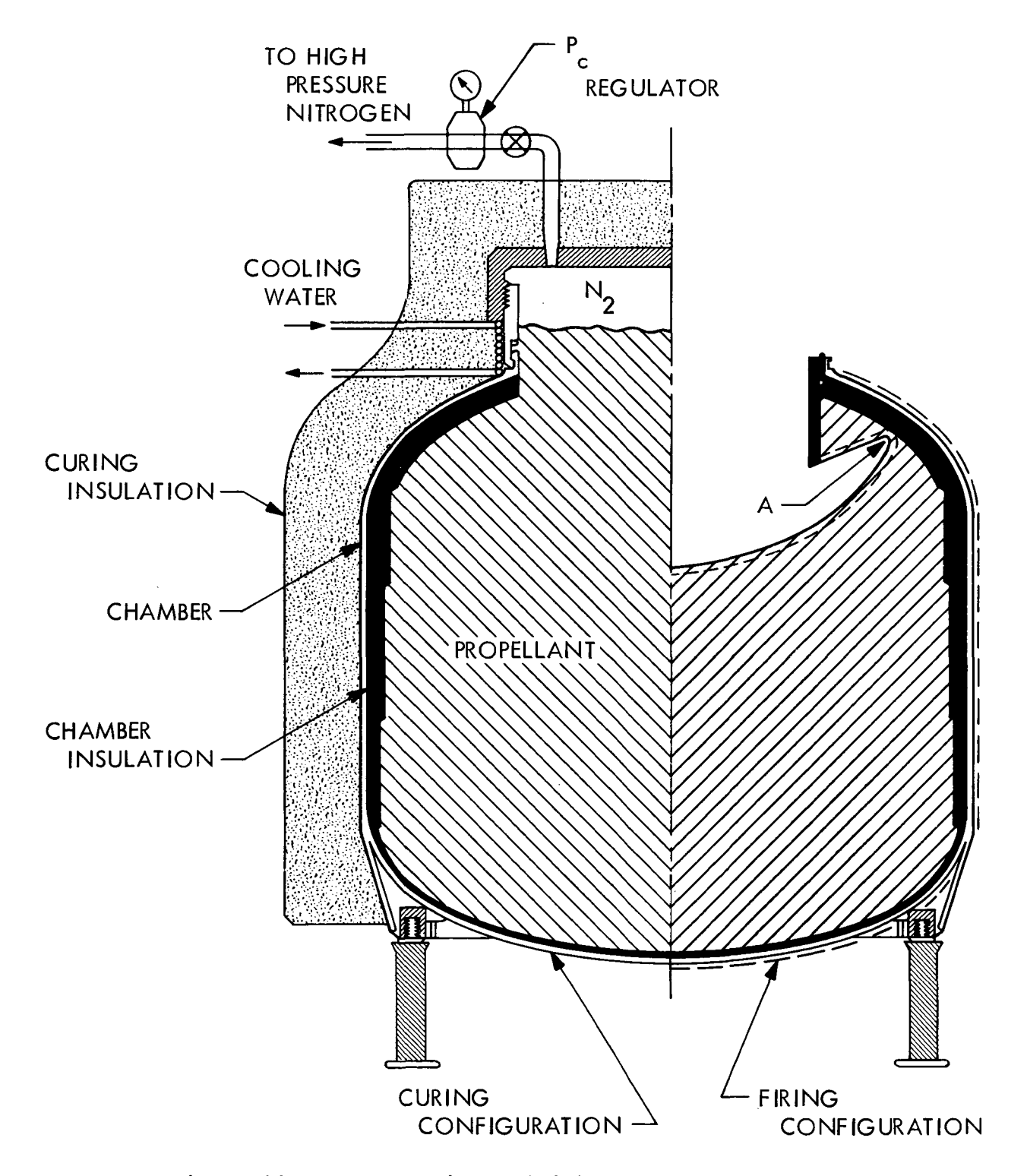


Figure 10. Motor curing and firing configurations

JPL Technical Memorandum 33-528

the center. Because there is a propellant shrinkage of about 1/2 to 1% during cure, a crack or cavity could form in the liquid center near or at the end of the curing stage and cause a failure later on firing.

Zone curing was proposed as a potential remedy. By circulating cooling water through copper coils around the top of the chamber (c.f. Figure 10, left side) and insulating all parts except the bottom, the cure would be accelerated at the bottom and the interface zone between cured and uncured propellant would gradually progress toward the top. As the propellant shrinks, it would draw on the reservoir of uncured propellant above so that cracking or voids, if any, would form near the top at the end of the cure. Later, that portion, containing any imperfections, would be trimmed out to make space for the nozzle (see Figure 10, right side). In practice no visible flaws have been observed.

The second failure mode could arise from the induced tension stresses from shrinkage on cure, from the much higher coefficient of contraction for the propellant than the chamber during the cool-down from the cure temperature, and from pressurizing the motor during firing. As the propellant contracts during cooldown from cure, or the chamber expands relative to the rigid nozzle attachment, the tension stresses in the propellant tend to break the insulation-propellant bond at point A (right side Figure 10), or create a crack down the center.

The remedy proposed was to cure at the maximum expected firing pressure,  $121 \text{ N/cm}^2$ , rather than the JPL-conventional  $34 \text{ N/cm}^2$ . Then the outside configuration of the propellant would be created

during cure (1) in the chamber-enlarged condition and (2) with the propellant in high compression and the chamber in high tension. Thus, during the critical cool-down from the cure temperature, the decrease in chamber volume as it is depressurized and cooled tends to offset much of the large contraction in the propellant volume as it cools. During cure, cooling water is circulated through the coils for only one day of the 4 to 6 day cure. Cool-down from cure and depressurization occur simultaneously over a 3-day period for the 25-kg motor and a 5-day period for the 355-kg motor; decrements of temperature and pressure are divided equally among the days.

1. <u>Feasibility Demonstration</u>. Table I indicates some experimental results. Two 25-kg motors, P83 and P67, were prepared using propellant JPL 540. Motor P83 was prepared with standard process techniques, 34 N/cm<sup>2</sup> and bulk cure; motor P67 was cured at 121 N/cm<sup>2</sup> and with zone cure.

In a simulation of static firings, the motors were pressurized to 190 N/cm<sup>2</sup> (i.e., 95% of the chamber proof pressure), held for 3 min, radiographed at pressure to check for flaws or failures, depressurized, and again radiographed. This procedure was carried out at each of the following temperatures: 22, 10, -12, -28, -46, and +74°C. They were then shock cycled after pressurization at +75°C directly to -54°C where they were again pressurized. Conditioning times at each temperature were a minimum of 3 days. Radiographic and visual inspection revealed no apparent flaws or failures.

Because both motors were unexpectedly available for further tests, it was decided to make a preliminary assessment of the creep properties for

TABLE I. PRESSURE TEST RESULTS ON CASE-BONDED END-BURNING MOTORS

	<del></del>	
CHARACTERISTIC	MOTOR P83	MOTOR P67
Propellant	JPL 540	JPL 540
Cure pressure (N/cm²)	34	121
Type cure	Bulk	Zone
Motor test pressure (N/cm <sup>2</sup> )	190	190
Motor test temperatures (°C)	22, 10, -12, -28,	22, -28, -46,
	-46 & +74	& +74
	(No failures)	(No failures)
Motor thermal shock temperatures (°C)	74 to -54	74 to -54
Propellant		
Maximum stress (N/cm2)	72	72
Strain at maximum stress (%)	160	160
Secant modulus (N/cm <sup>2</sup> )	45	45
Creep tests		
Nozzle end down at 79°C	Slumped after 5 days	
Nozzle end up at 22°C		Negligible creep after 1 year

the end burning configuration; the propellant secant modulus (about  $45 \text{ N/cm}^2$ ) on this batch was unusually low.

After 5 days in the inverted position, nozzle end down at 79°C, motor P83 rapidly deformed or slumped. See Figure 11 for the motor before and after the test. Motor P67 was stored nozzle end up at room temperature for one year. Deformations at that time were found to be negligible. Thus, the tests bounded the area of interest.

Neither of the two motors could have been static fired because they utilized chambers that had been insulated for radial burning charges for a different purpose; for this application there was insufficient insulation to prevent a chamber burn-through.

To demonstrate feasibility of the case-bonded concept for the entire burning period rather than for the initial geometry alone, it was necessary to static fire flight-weight case-bonded end-burning motors.

Table II summarizes some motor characteristics and Table III the static firing results for the next group of 3 motors. Motor P78 was used to demonstrate technical feasibility in the 25-kg size. Motor P45 was a small scale precursor for the demonstration firing, D-0, of technical feasibility at the 355-kg size.

Motor P45 was cast deliberately with a lower propellant elongation than P78, closer to that expected in the large motor and fired with a nozzle designed to produce its lower chamber pressure. During charge trimming to contour, the ring of propellant in the aft dome exhibited bond weakness to the insulation and partial separation, but the cause may have been due to a processing error during curing (i.e., a 3- rather than 1-day water cooling of the motor aft end) rather than basic inadequacy of the propellant





Figure 11. Before and after slump of inverted motor at 79°C

CHARACTERISTICS OF CASE-BONDED END-BURNING MOTORS FOR FEASIBILITY TESTS TABLE II.

Motor Propellant (JPL 540)         60         60         60           Cure temperature (°C)         Cure type         Zone cure         Zone cure           Cure pressure (N/cm²)         121         121         121           Maximum tensile strength (N/cm²)         139         85         129           Elongation at maximum stress (%)         37.3         120         87           Elongation at maximum stress (%)         37.3         120         68           Propellant weight (kg)         25.8         25.7         129           Chamber         410 Chrome steel         410 Chrome steel         414 V Titanium           Proof pressure (N/cm²)         32.5         32.5         71.0           Diameter (cm)         30.6         30.6         71.0           Weight (kg)         1.0 to 0.5         1.0 to 0.5         11.0 to 0.25           Weight (kg)         3.28         3.19         17.0           Nozzle (Submerged; Phenolic/Carbon         1.0 to 0.5         1.0 to 0.5         17.0           Aparasion ratio         2.15         2.30         10.43	CHARACTERISTIC	25 kg (P78)	25 kg (P45)	355 kg (T10)
2 Cone cure 2 Cone cure 3 121 121 122 139 85 37.3 25.8 25.7 25.8 32.5 30.6 1.74 11.78 11.78 115.5 115.5 25.30 25.30	Motor Propellant (JPL 540)			
Zone cure 121 52 139 37.3 25.8 410 Chrome steel 200 32.5 30.6 1.74 1.0 to 0.5 15.5 3.310 2.15 2.15 2.15	Cure temperature (°C)	09	09	09
121 52 139 37.3 25.8 410 Chrome steel 200 32.5 30.6 1.0 to 0.5 1.0 to 0.5 1.0 to 0.5 1.15.5 1.174 1.174 1.178 1.	Cure type	Zone cure	Zone cure <sup>a</sup>	Zone cure
139 37.3 25.8 25.7 410 Chrome steel 200 32.5 30.6 1.74 1.0 to 0.5 1.0 to 0.5 3.28 3.310 2.30 2.30	Cure pressure (N/cm²) Maximum tensile strength (N/cm²)	121	121	121 87
37.3 25.8 25.7 410 Chrome steel 410 Chrome steel 200 32.5 30.6 1.74 1.0 to 0.5 1.0 to 0.5 1.15.5 1.1	Elongation at maximum stress (%)	139	85	129
25.8 25.7 410 Chrome steel 410 Chrome steel 200 32.5 30.6 1.74 1.78 1.0 to 0.5 3.28 1.0 to 0.5 3.28 1.0 to 0.5 3.28 1.0 to 0.5 3.28 1.0 to 0.5 3.28 2.19	Secant modulus (N/cm <sup>2</sup> )	37.3	120	89
410 Chrome steel 200 200 32.5 32.5 30.6 1.74 1.78 1.0 to 0.5 3.28 3.310 3.310 2.15 2.30	Propellant weight (kg)	25.8	25.7	353
410 Chrome steel 200 200 32.5 32.5 30.6 1.74 1.78 1.0 to 0.5 3.28 3.19 15.5 3.310 2.15 2.30	Chamber			
200 32.5 30.6 1.74 1.0 to 0.5 3.28 1.0 to 0.5 3.28 1.0 to 0.5 3.19 15.5 15.5 14.1 2.15 2.30	Type	410 Chrome steel	410 Chrome steel	6Al 4V Titanium
32.5 30.6 1.74 1.0 to 0.5 3.28 1.0 to 0.5 3.19 15.5 14.1 3.310 2.15 2.30	Proof pressure (N/cm <sup>2</sup> )	200	200	155
1.0 to 0.5 1.0 to 0.5 3.28 15.5 16.5 178 1.0 to 0.5 3.19 3.19 3.310 2.30	Length (cm)	32.5	32.5	71.0
1.0 to 0.5 3.28 3.28 3.19 15.5 3.310 2.15 2.30	Weight (kg)	30.0 1.74	30.6	71.0 11.08
1.0 to 0.5 3.28 3.28 3.19 15.5 14.1 2.15 2.30				
1.0 to 0.5 3.28 3.28 3.19 15.5 14.1 3.310 2.15 2.30	Insulation (Gen-Gard V-52)			
3.28 3.19 15.5 14.1 3.310 3.765 2.15 2.30	Thickness (cm)	1.0 to 0.5	1.0 to 0.5	1.0 to 0.25
15.5 3.310 2.15 14.1 3.765 2.30	Weight (kg)	3.28	3.19	17.0
15.5 3.310 2.15 14.1 3.765 2.15	Nozzle (Submerged; Phenolic/Carbon			
15.5 3.310 2.15 14.1 3.765 2.30				
3.310 2.15 2.30	Expansion ratio	15.5	14.1	11.0
	Tiffoat diameter (Cm) Weight (kg)	3.310 2.15	3.765	9.000

<sup>&</sup>lt;sup>a</sup>Propellant ring in chamber aft dome exhibited bond weakness and slight separation from insulation — perhaps due to abnormal zone curing. Void filled with epoxy resin and resin cured before firing.

TABLE III. STATIC FIRING FEASIBILITY TESTS OF CASE-BONDED END-BURNING MOTORS

	CASE-BONDED END-BURNING MOTORS	ED END-BUR	INTING MOTOR	g	
PARAMETER	27 kg SYNCOM <sup>a</sup> (Reference)	25 kg (P78)	25 kg (P45)	345 kg ATSa (Reference)	355 kg (T10)
Test date	Oct. '62	Feb. 169	Mar. '69	Aug. '66	May '69
Motor temperature (°C)	15	15	15	15	15
Type of test	Horizontal	Horizontal	Horizontal	Horizontal spin	Vertical
Action time (s)	19.55	39.4	48.2	42.5	110.0
Mean effective pressure (N/cm <sup>2</sup> )	136	123	69	142	76.0
Maximum pressure (N/cm <sup>2</sup> )	178	136	81	180	94.0
Propellant c* (m/s) <sup>b</sup>	1499	1498	1471	1515	1511
Average mass flow rate (kg/s)	1.41	0.654	0.532	8.11	3.21
Change in throat area (%)	0.5 to 1.5	1.5	2.0	1.5	0.3
Weight of Al <sub>2</sub> 0 <sub>3</sub> slag (kg)	Trace	0.02	0. 13	Trace	Trace

<sup>a</sup>From motor qualification data. <sup>b</sup>Based on loaded propellant weight and average throat area.

mechanical properties. The void in the separated region was repaired by filling with epoxy resin, the resin was cured, and the motor successfully static fired.

In Table III, the results for the 25-kg Syncom and 345-kg ATS radial burning motors are included for comparison. All end-burning motors were zone cured at  $60^{\circ}$ C under  $121-N/cm^2$  pressure.

As desired, action times for the 3 motors were 2 to 2-1/2 times as long as those of the radial burning reference motors. Despite the longer burning times, the increases in the throat area of the high density graphite inserts were quite acceptable.

The propellant characteristic velocity, c\*, for motors P78 and T10 seemed unaltered from those of their radial burning reference motors despite the lower pressures. However, in motor P45 the c\* dropped about 1.8%, presumably because of the combination of very low pressure, 69 N/cm<sup>2</sup>, and small motor size.

In both reference radial-burning motors, the weight of the aluminum oxide slag or residue had been negligible. In P78, the first end-burner, there was a small amount, but in P45 a pronounced puddle formed in the bottom of the motor. Chemical analysis revealed that over 60% of the slag was unburned aluminum, a plausible explanation for its low c\* value.

The longer burning time of the large demonstration motor T10 might permit slag to pyrolyze the chamber insulation locally (a condition which exists during static firing but not in space operation) and burn a hole in the chamber; therefore, it was decided that T10 would be fired vertically nozzle end up, so that the combustion gases would entrain any condensing slag. If, in subsequent 25-kg motor firings the slag problem persisted, it was believed

that the problem might be resolved by converting to an external nozzle although at a slight penalty in motor length.

It was concluded that, with the successful firing of these three motors: (1) technical feasibility of the concept of case-bonded end-burning charges without mechanical stress relief in the 25- and 355-kg class had been demonstrated; (2) propellant c\* in large motor firings appeared to be unaffected even at a pressure as low as  $76 \text{ N/cm}^2$ ; however,  $I_{\text{sp}}$  efficiency had yet to be checked. In small motors with propellant JPL 540, the c\* appears to be dropping off at a pressure of about  $70 \text{ N/cm}^2$ ; (3) a propellant secant modulus of  $120 \text{ N/cm}^2$  may be marginal for case-bonded end-burners with the processing techniques used (see Table II).

2. Lower Propellant Burning Rate and Motor Processing. Propellant JPL 540 had been adopted at the beginning of the program because of its unusually good mechanical properties, but adopted only until a propellant with a lower burning rate could be made available. The JPL Saturethane propellant, a urethane-cured saturated hydrocarbon-ammonium perchlorate system under development for heat sterilizable motor applications, had the very low burning rate desired — 0.23 versus 0.35 cm/s at 69 N/cm<sup>2</sup>. Despite its higher modulus, lower elongation, and higher cure temperature (88°C), efforts were oriented toward utilizing the Saturethane propellant and determining whether zone curing at high pressure was better than the standard bulk cure at 34 N/cm<sup>2</sup>.

Table IV summarizes the characteristics for 5 motors from 2 batches of Saturethane propellant. The chamber insulation was the improved ethylene propylene type, Gen-Gard 4010, a precursor and slightly modified version of the ethylene propylene class finally adopted, Gen-Gard 4030, rather than the butadiene acrylonitrile Gen-Gard V-52 used previously.

TABLE IV. CHARACTERISTICS OF CASE-BONDED END-BURNING MOTORS USING SATURETHANE PROPELLANT

		NE PROPEI			
PURPOSE ──◆ F	EVALUATE ZONE - HI	HIGH PRESSURE CURE	EVALUATE SA	SATURETHANE F	PROPELLANT
BATCH NO.	JS-51	JS-51	JS-50	JS-50	JS-50
MOTOR	P84	P96	P102	P103	P85
CHARACTERISTIC					
Propellant (Saturethane)					
Type Designation	Very high modulus XS-6	Very high modulus XS-6	High modulus XS-54	High modulus	High modulus
Flame temperature (°C) Cure temperature (°C)	2584 88	2584	2584	2584	2584
Cure type	Bulk	Zone	Zone	Zone	Zone
Cure pressure (N/cm²) Maximum tensile strength (N/cm²)	34 218	121 218	190 136	190 136	190 136
Elongation at maximum stress (%) Secant modulus (N/cm <sup>2</sup> ) Propellant weight (kg)	53 652 	33 652 	48 284 23.9	48 284 23.6	48 284 23.5
Chamber (410 Chrome Steel)					
Proof pressure (N/cm <sup>2</sup> )	200	200	200	200	200
Length (cm)	32.5	32.5	32.5	32.5	32.5
Diameter (cm) Weight (kg)	1.76	30.0 1.74	30.6 1.78	30.6 1.75	30.6 1.77
Insulation (Gen-Gard 4010)a					
Thickness (cm) Weight (kg)	0.66 to 0.25 1.93	0.66 to 0.25 1.86	0.66 to 0.25 1.84	0.66 to 0.25 1.79	0.66 to 0.25 1.85
Nozzle (Carbon Cloth-Phenolic)					
Type	1 1	1 1	Submerged	Submerged	External
Throat diameter Weight (kg)	Unfired 	Unfired	2.855 2.08	20. 2 2. 861 3. 14	2.857 3.64b
t :- 0 ()					
Kesuit (On Cooling From Cure)	Severe propellant-insulation separation in nozzle dome.	-insulation sle dome.	Some propellant-insulation Propellant in most of nozzl removed and motors fired.	Some propellant-insulation separation. Propellant in most of nozzle dome removed and motors fired.	ration. me

<sup>a</sup>Ethylene propylene terpolymer rubber base with silica and/or asbestos filler supplied by General Tire and Rubber Co. <sup>b</sup>Includes weight of adapter for external nozzle. The earlier effort to differentiate between the standard bulk cure and zone cure at high pressure using the low modulus JPL 540 had resulted in both motors passing even the severest test (see Table I). Therefore, the propellant in the first batch for motors P84 and P96 had been tailored deliberately to have a very high modulus. Its high modulus, in association with the greater propellant contraction from its higher cure temperature, would aggravate the tension stresses on cooling from cure and insure failure, hopefully, of one of the two motors. Indeed stresses were sufficiently severe that both charges separated in the nozzle dome at the propellant-insulation interface by about 0.5 cm. No attempt was made to patch and fire the motors.

In the second batch of three motors, P102, P103, and P85, the propellant modulus was decreased as much as binder tailoring in the Saturethane formulation would permit and the cure pressure raised from 121 N/cm<sup>2</sup> to 190 N/cm<sup>2</sup> in an effort to process motors successfully with Saturethane propellants. Although the propellant-insulation separation was markedly reduced, it was not eliminated.

Subsequent tests of the elevated temperature bond strength of Saturethane propellant to Gen-Gard 4010 insulation revealed that its bond was much poorer than for propellant JPL 540 to either insulation Gen-Gard 4010 or V-52 as indicated in the following:

Peel Strength at Temperature

Propellant/Insulation	22°C	43°C	60°C
Saturethane/Gen-Gard 4010	350 cm-N	101 cm-N	negligible
JPL 540/Gen-Gard 4010	451 cm-N		158 cm-N
JPL 540/Gen-Gard V-52	259 cm-N		113 cm-N

Thus, on cooling from the 88°C cure, tension and/or shear stresses at the Saturethane propellant-4010 insulation interface had developed at high enough temperature that the poor bond strength was exceeded. The JPL 540/V-52 combination, of course, withstood the cool down from a 60°C cure successfully in motors P78, P45 and T10 discussed earlier.

By removing the separated portion of the propellant (about 2 kg each) from the aft domes of the motors P102, P103, and P85, all three could be static fired. The results are summarized in Table V. Data for the radial burning 27-kg Syncom motor are included for comparison. Burning times, as expected, were substantially longer than for earlier motors. The first two, with submerged nozzles, produced abnormally large amounts of aluminum oxide/aluminum slag (about 0.65 kg) probably because of the low flame temperature of this propellant (theoretically 2584°C). The vacuum specific impulse, not surprisingly, was quite low, 2520 N-s/kg, at an expansion ratio of 50.

In an effort to see whether the slag could be eliminated and the vacuum specific impulse improved, motor P85 was fired with an external nozzle. The amount of resultant slag was reduced, 0.24 kg, but not eliminated. The specific impulse, although slightly higher (2560 N-s/kg) than the motor with the submerged nozzle, was still very low.

About that time concurrent propellant development work to reduce propellant burning rate had confirmed that a coarse oxidizer with a trimodal particle size distribution would decrease the burning rate of the polyurethane propellant JPL 540 to a rate not much higher than Saturethane. Because of the limited mechanical properties and unfavorable ballistic results from Saturethane propellant, work was discontinued on the latter in favor of JPL 540 (Trimodal) (see Table VI).

STATIC FIRING RESULTS OF CASE-BONDED END-BURNING MOTORS WITH SATURETHANE PROPELLANT TABLE V.

PARAMETER	27 kg SYNCOM <sup>a</sup> (Reference)	P102	P103	P85
Test date	Oct. '62	July 169	July '69	Nov. '69
Motor temperature (°C)	15	15	15	15
Propellant	JPL 540	Saturethane	Saturethane	Saturethane
Type of test	Horizontal	Vertical nozzle down	Vertical nozzle down	Vertical nozzle down
Action time (s)	19.55	65.8	63.4	64.4
Mean effective pressure (N/cm <sup>2</sup> )	136	89.6	90.4	102.9
Maximum pressure (N/cm <sup>2</sup> )	178	107.7	105.3	119.5
Maximum thrust (N)	1 1	1 1	1051	1077
Propellant c* (m/s) <sup>b</sup>	1499	1482	1452	1451
Average mass flow rate (kg/s)	1.41	0.382	0.383	0.374
Change in throat area (%)	0.5 to 1.5	-1.77	-4.2	16.8
Weight of Al <sub>2</sub> 0 <sub>3</sub> slag (kg)	Trace	0.68	0.64	0.24
$Vac Isp (\epsilon = 50) (N-s/kg)$	2805	Atmospheric	2521	2560
		3111		

<sup>b</sup>Based on loaded propellant weight and average throat area. <sup>a</sup>From motor qualification data; radial burning design.

TABLE VI. CHARACTERISTICS OF CASE-BONDED END-BURNING MOTORS USING JPL 540 (TRIMODAL) PROPELLANT

PURPOSE	EVALUATE	ATE CURE AND VACUUM Isp	uum I <sub>sp</sub>
BATCH NO. ─	EB-9	EB-9	EB-9
MOTOR ─	P78(2)	P99	P50
CHARACTERISTIC			
Propellant			
Designation	XS-65	XS-65	XS-65
Flame temperature (°C)	2904	2904	2904
Cure temperature (°C)	09	09	09
Cure type	Zone	Zone	Bulk
Cure pressure $(N/cm^2)$	121	121	34
gth (N	128	128	128
Elongation at maximum stress (%)	140	140	140
Secant modulus (N/cm <sup>2</sup> )	91.4	91.4	91.4
Propellant weight (kg)	•	26.64	
Chamber (410 Chrome Steel)			
Proof pressure $(N/cm^2)$	200	200	200
Length (cm)	32.5	32.5	32.5
Diameter (cm)	30.6	30.6	30.6
Weight (kg)	2.01	1.94	1.86
Insulation (Gen-Gard 4010a)			
Thickness (cm)	0.66  to  0.25	0.66 to 0.25	0.66 to 0.25
Weight (kg)	1.85	1.83	1.83
Nozzle (Carbon Cloth-Phenolic)			
Type	No firing	No firing	No firing
Result (On Cooling from Cure)	Chamber buckled	Chamber buckled	Chamber buckled
	somewhat	somewhat	severely

 $^{\mathrm{a}}\mathrm{Ethylene}$  propylene terpolymer rubber base with silica and/or asbestos filler supplied by General Tire and Rubber Co.

Motors from batch EB-9 using JPL 540 (Trimodal) propellant resulted, on cooling from the 60°C cure temperature, in buckling of the thin-walled (0.030 cm) cylindrical section of the chamber — severely in the case of the motor with the standard JPL cure, and only slightly for the charges zone cured at 121 N/cm<sup>2</sup> (see Figure 12). Radiographic inspection revealed minor separation between the propellant and insulation in the buckled region of P50 so no attempt was made to static fire.

A review of all available data at that point indicated that three changes appeared desirable: (1) an increase in the pressure during propellant curing; (2) a further lowering of the propellant modulus at the expense of tensile strength, and (3) more reproducible propellant mechanical properties for a given formulation. The latter two will be discussed in the next section on propellant development.

The pressure to be used for cure was determined from a simple analysis of the volume changes of the propellant and chamber respectively during depressurization and cool-down from the cure temperature assuming that the two volume changes should be equal at ambient temperature and atmospheric pressure. Volume changes for the 25-kg chrome steel motor and the 355-kg titanium motor are as follows (a minus sign indicates a decrease in volume):

	410 Cr Steel 25-kg Chamber	Titanium 355-kg Chamber
Total chamber volume	$18,853 \text{ cm}^3$	$239,500 \text{ cm}^3$
Depressurization \\ \text{from 190 N/cm <sup>2</sup> } \\ \text{from 134.8 N/cm <sup>2</sup> }	-205 cm <sup>3</sup>	-2555 cm <sup>3</sup>
Propellant expansion from 190 N/cm <sup>2</sup> with depressurization from 134.8 N/cm <sup>2</sup>	+10.3 cm <sup>3</sup>	+93.0 cm <sup>3</sup>
Propellant thermal shrinkage (cooling from 60° to 15°C)	-226 cm <sup>3</sup>	-2916 cm <sup>3</sup>
Case thermal shrinkage (cooling from 60° to 15°C)	-24.9 cm <sup>3</sup>	-281 cm <sup>3</sup>
Amount case volume change exceeded propellant volume change	+14.2 cm <sup>3</sup> (i.e., some net compression)	+13 cm <sup>3</sup> (i.e., some net compression)

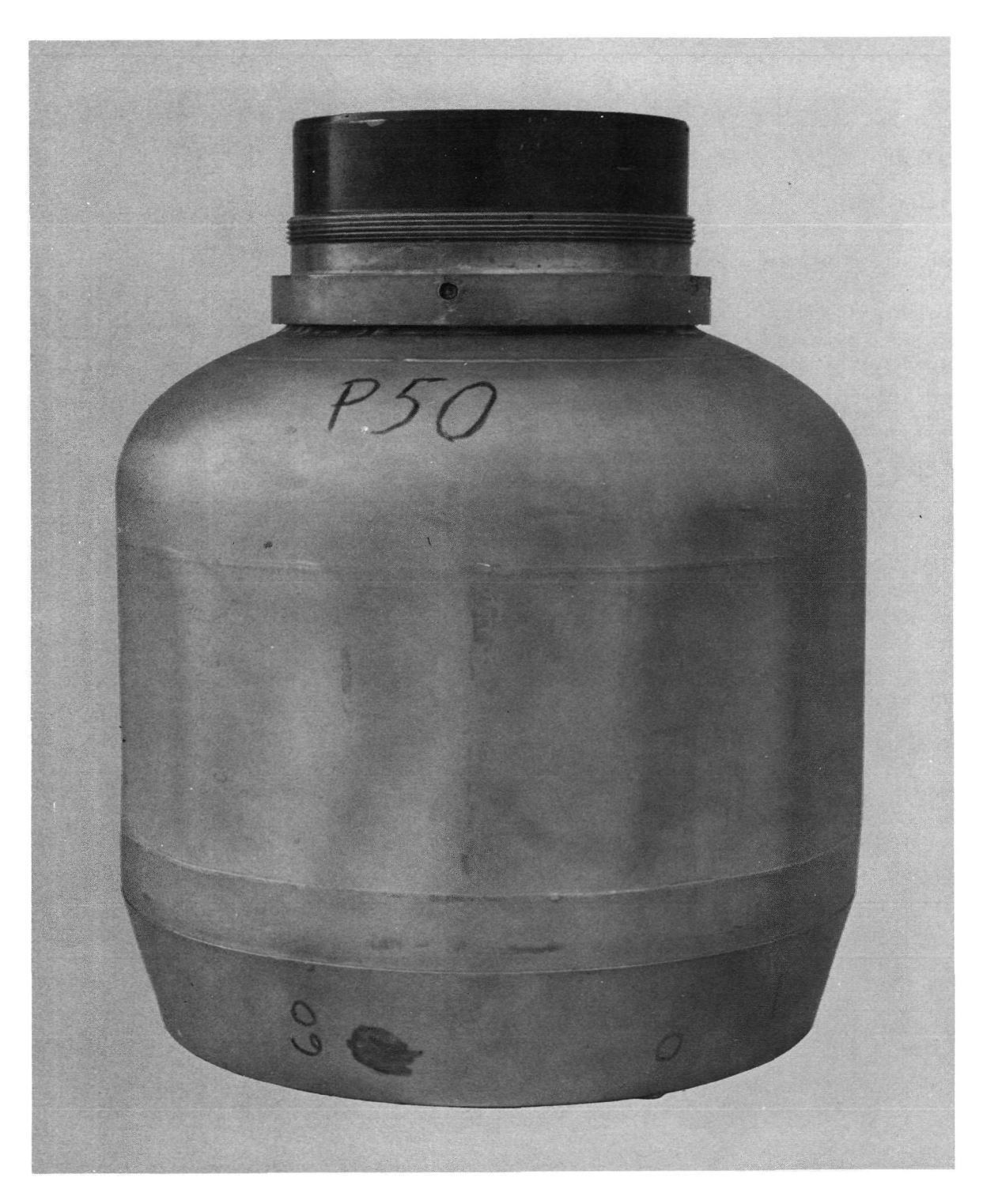


Figure 12. Buckled chamber after cooling from cure temperature

In a broad sense the procedure minimizes the relative motions of propellant and insulation to avoid shear failure at the propellant interface at high temperature when the bond is weakest while maintaining compression loads throughout cool-down to avoid buckling the thin chamber wall.

The stress analysis in Ref. 5 for the JPL case-bonded end-burning motor design, using a finite element technique and elastic analysis, indicates some interesting trends and sensitivities to changing parameters; the authors note also that difficulties may be encountered with chamber buckling at low temperatures.

Propellant Tailoring. Reference 6 reports on the propellant formulation work associated with the mechanical properties requirements of the case-bonded end-burner; it builds on earlier propellant formulation studies at JPL. Figure 13 summarizes the work in the plot of propellant maximum tensile strength, S<sub>m</sub>, versus percentage of elongation at maximum stress. For reference, the box in the upper left bounds, approximately, the properties provided by current propellants.

The JPL 500 curve indicates the properties that the early family of polyether polyurethanes possessed. The properties of the entire family were markedly upgraded twice. First, when a surface active agent, Geigy's Alrosperse 11P, was incorporated to give the JPL 535 family of propellants, and second, when aluminum was added to the formulations to give the JPL 540 group, the family available at the beginning of the end-burner program.

In tailoring the propellant family for case-bonded end-burners, an assessment of processing results of Tables I, II, and IV produced the tentative range of mechanical properties shown in Figure 13 as a target or goal for the work. Polymer network theory was used to adjust the binder molecular structure, and a propellant family with higher elongations and lower

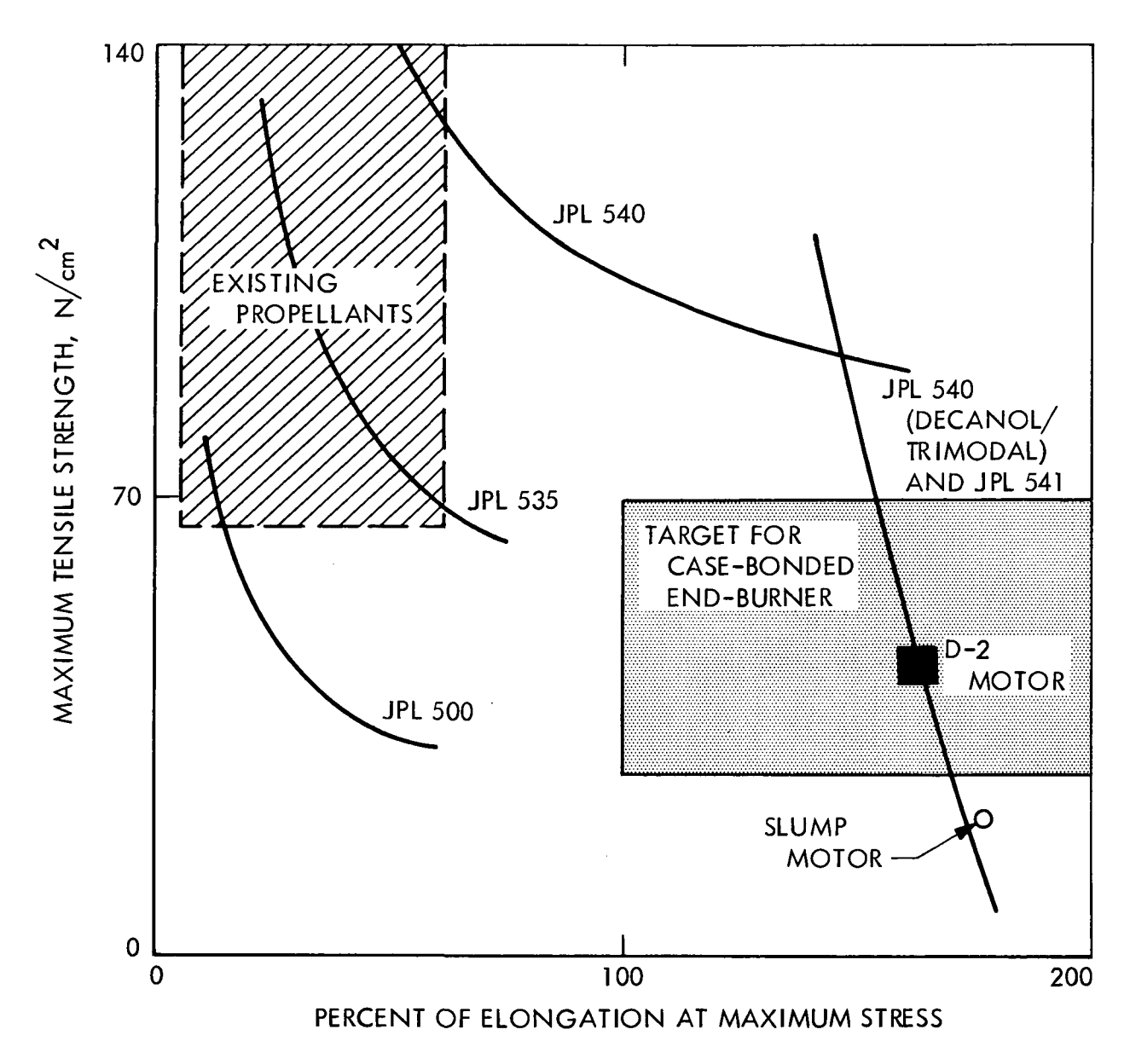


Figure 13. Tailoring propellant mechanical properties

moduli was soon obtained — the JPL 540 (Decanol/Trimodal) and, subsequently, the JPL 541 class with 2-1/2% oxamide incorporated. This was accomplished by introducing a monofunctional alcohol, decanol (C<sub>10</sub>H<sub>21</sub>OH), which effectively lowered the polymer crosslink concentration, and provided internal binder plasticization, resulting in propellants well within the boxed region of mechanical properties believed to be desirable.

A special modification of the JPL 540 (Decanol/Trimodal) that had unusually low modulus was prepared also for slump motor tests to be described later (c.f. Figure 13). Reproducibility of the mechanical properties for a given propellant appears to be much improved by the use of the formulation technique adopted.

Independent efforts to lower the burning rate of JPL 540 led to two significant reductions: (1) the use of coarse trimodal oxidizer (16%, 50 micron; 34%, 200 micron; 50%, 400 micron), and (2) substitution of 2-1/2% oxamide (NH<sub>2</sub>COCONH<sub>2</sub>) for oxidizer and binder in equal proportions, designated JPL 541 and capable of meeting the burning rate requirements of motor D-2. The burning rate-pressure relationships for both are shown in Figure 8; values are based on Crawford bomb measurements as predicted for 355-kg motor firings.

## Modified Propellant Processing with Mono-Alcohol-Modified Propellant. Because it was believed that the higher cure pressure of 190 N/cm<sup>2</sup> advocated for the 25-kg steel chamber would prevent the buckling experienced with motors P78 (2), P99, and P50 during cooldown from the cure temperature, two new motors, P33 and P97, were cast as case-bonded end-burners with the much higher cure pressure. Motor P33 would then be fired at the maximum expected design pressure to determine whether the case-bonded charge could withstand the high chamber strain. Motor P97

was intended for a propellant vacuum specific impulse measurement but later was reassigned to a feasibility demonstration of the all-carbon nozzle (see Table VII). Independent laboratory tests to determine the effect of increasing cure pressure on the propellant mechanical properties of vacuum-cast, well-consolidated propellant had shown no measurable effect. Later, motors P64 and P55 were also cast for additional all-carbon nozzle tests using the high cure pressure.

Propellant EB-31 from the early formulation studies on JPL 540 (Trimodal) modified with decanol looked promising at that time, and was adopted as added insurance of success. As expected, all four motors cooled to 15°C from the cure temperature without any signs of buckling.

Later, work with decanol as a binder modifier resulted in propellants with even lower modulus — in the middle of the range of mechanical properties believed to be desirable for case-bonded end-burners, EB-27 and JPL 541. The former was used successfully in the high L/D motor tests and in the D-1 demonstration motor firing; the latter was used in the D-1A demonstration firing discussed late in the report.

Table VIII summarizes the static firing results for motors P33, P64, P97 and P65. Except for P65 and P97, instrumentation during the firings was kept to a bare minimum; only an oscillograph recorder was used because of the risk of motor failure. In P33 and P64 the charge was exposed to the strain associated with the pressures of 196 and 197 N/cm<sup>2</sup> or 98% of the chamber proof pressure; calculated chamber hoop stress was 98,400 N/cm<sup>2</sup>. Neither charge appeared to crack or separate but interpretation of the data was, and is usually, complicated by unpredictable aluminum oxide deposition on the nozzle throat early in the firing of the small 25-kg motors. Confidence

TABLE VII. CHARACTERISTICS OF CASE-BONDED END-BURNING MOTORS USING JPL 540 (TRIMODAL) MODIFIED WITH DECANOL

PURPOSE —	CHECK B AFTER PRESSUF	CHECK BUCKLING AFTER HIGHER PRESSURE CURE	FIRST FIRING OF ALL-CARBON NOZZLE	THIRD FIRING OF ALL-CARBON NOZZLE
BATCH NO. ─◆	JS-52	JS-52	BD-117	BD-120
MOTOR —	P33	P97	P64	P 55
CHARACTERISTIC				
Propellant JPL 540 (Decanol/Trimodal)				
Designation	EB 31	EB 31	EB 31	EB 31
Flame temperature (°C)	2904 60	2904 60	2904	290 <del>4</del> 60
Cure type	Zone	Zone	Zone	Zone
Cure pressure (N/cm <sup>2</sup> )	190	190	190	190
Maximum tensile strength (N/cm²)	86	86 1 5 3	103	86
Secant modulus $(N/cm^2)$	56	56	64	265
Propellant weight (kg)	25.95	25.42	26.65	26.65
Chamber (410 Chrome Steel)				
Proof pressure $(N/cm^2)$	200	200	200	200
Length (cm)	32.5	32.5	32.5	32.5
Diameter (cm)	30.6	30.6	30.6	30.6
Weight (kg)	1.05	1.94	1.79	1.75
Insulation (Gen-Gard 4010a				
Thickness (cm)	1.0 to 0.5	1.0 to 0.5	0.66 to 0.25	0.66 to 0.25
Weight (kg)	2.66	2.82	1.89	1.81
Nozzle				
Type	Carbon	All-carbon	All-carbon	All-carbon
	clotn/ phenolic			
Result (On Cooling from Cure)	No buckling	No buckling	No buckling	No buckling

 $^{\mathrm{a}}\mathrm{Ethylene}$  propylene terpolymer rubber base with silica and/or asbestos filler supplied by General Tire and Rubber Co.

STATIC FIRING RESULTS FOR CASE-BONDED END-BURNING MOTORS USING JPL 540 (TRIMODAL) MODIFIED WITH DECANOL TABLE VIII.

PARAMETER	P33 TEST CHARGE AT MAXIMUM STRAIN	P64 FIRST TEST OF ALL- CARBON NOZZLE	P97 SECOND TEST OF ALL- CARBON NOZZLE	P55 ALTITUDE TEST OF ALL-CARBON NOZZLE AND PROPELLANT I sp
Test date	Jan. '70	Mar. '70	Aug. 170	Oct. '70
Motor temperature (°C)	22	22	22	22
Action time (s)	45	45	44	46
Mean effective pressure (N/cm <sup>2</sup> )	156	Not taken	120	126
Maximum pressure $(N/cm^2)$	196	197	146	158
Propellant $c^*$ (m/s)	1465	Not taken	1454	1478
Average mass flow rate (kg/s)	0.576	0.592	0.577	0.579
Change in throat area (%)	2.6	7.6	5.1	2.6
Vacuum specific impulse (Ns/kg)	Not taken	Not taken	Not taken	2637

that there were no charge failures was enhanced later with the firing of the 355-kg motors D-1 and D-1A.

The propellant c\* for motors P33, P97, and P55 was about 1.5 to 3% lower than usual; this may be due to the lower accuracy of the instrumentation of these tests, or the very coarse oxidizer used to lower the propellant burning rate. Reference 7 reports a small reduction in motor performance with increasing oxidizer particle size. Note, however, that in the large motor D-1 firing with propellant using coarse oxidizer the c\* was normal. The vacuum specific impulse on motor P55 was also low, about 2.5%. Separate calculations show that the I<sub>sp</sub> loss does not stem from the use of the all-carbon nozzles (see later section Nozzles for Long Burning Motors). It is tentatively concluded that a loss in I<sub>sp</sub> in 25-kg motors results from the use of coarse oxidizer in the propellant.

Pressure Tests of High L/D Motor. When the spacecraft envelope for propulsion permits, end-burning motors with chambers having a higher L/D than one can provide even lower thrust-to-mass ratios than one. Indeed this can be done using propellants with faster, more conventional burning rates than those under consideration — including the berylliumized propellants. However, as chamber L/D increases, the strains imposed on the propellant in this essentially triaxial stress field also increase. With the new availability of the low modulus propellant developed for the D-1 demonstration motor it became desirable to determine whether case-bonded end-burners with a high L/D were feasible.

A salvaged fully-annealed titanium chamber from the Explorer program, 15.4 cm in diameter by 91 cm long, was loaded with propellant EB-27, zone cured under 430  $\text{N/cm}^2$  at 60°C, cooled to room temperature, then trimmed to the contour shown in Figure 14. Incidentally, the stiff mounting ring

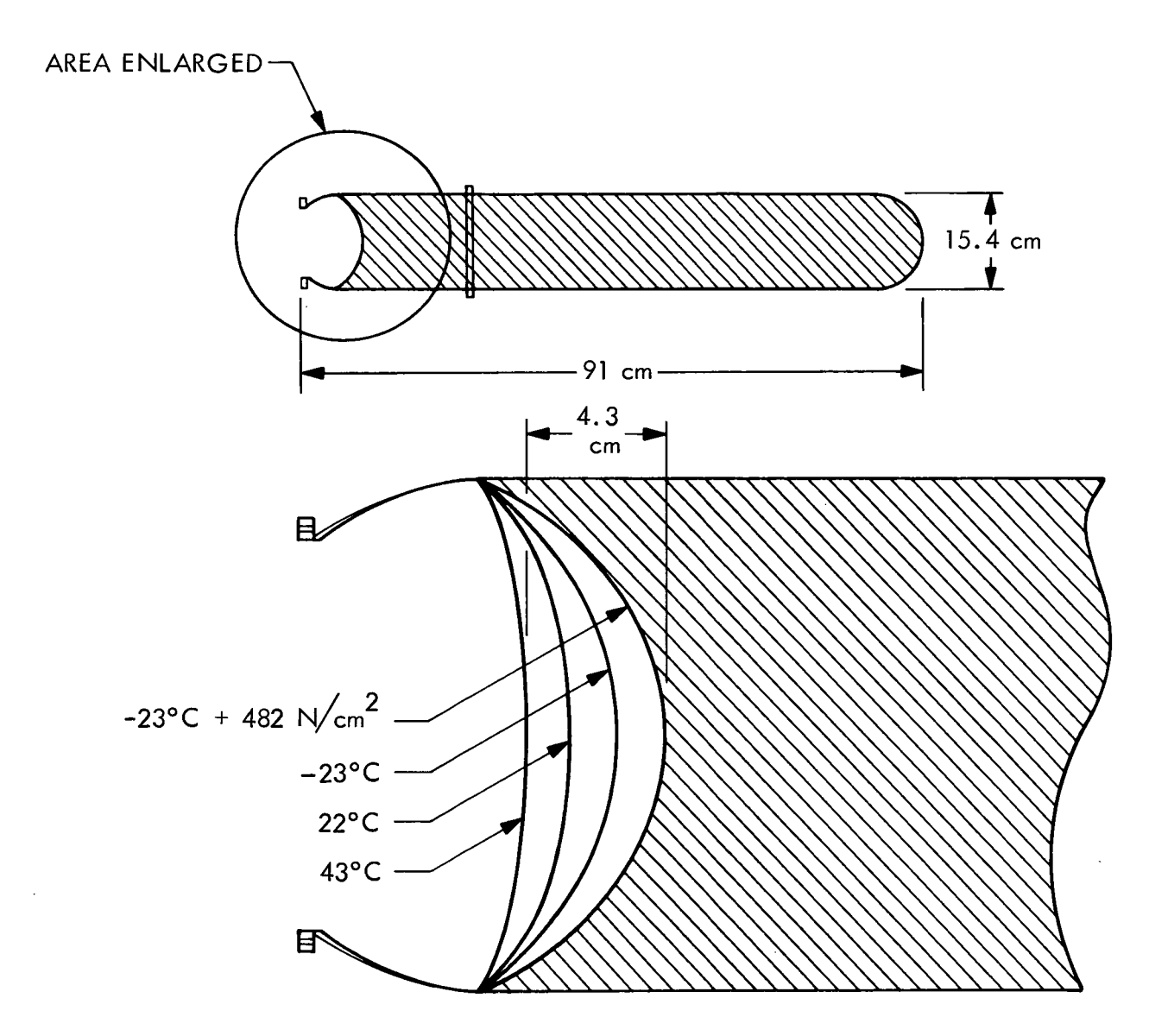


Figure 14. Propellant surface displacements in high L/D motor

23 cm from the nozzle end complicates the stresses locally but should affect the over-all test very little. The chamber is referred to as a case with an L/D of 5 to allow for its effect. The cured propellant had a tensile strength of 43 N/cm<sup>2</sup> and elongation at maximum stress of 145%. The cure pressure was selected such that on cooling from the cure temperature, the contraction in propellant volume just matches the change in case volume from depressurization and cooling as mentioned earlier.

The trimmed motor was pressure tested in a simulated firing at 480 N/cm<sup>2</sup> for at least 3 min, radiographed for flaws or propellant-insulation separations, depressurized and reradiographed at each of the following temperatures: 22°, 4, -12, -23 and 43°C. Figure 14 displays tracings from radiographs showing the position of the propellant at high, ambient, and low temperature and also at full pressure at -23°C. Maximum displacement of the surface was 4.3 cm yet no failures were observed.

The calculated volume change from the surface displacements on the radiographs agreed well with those calculated from the known coefficients of expansion for the propellant and titanium thus confirming that no separations between charge and chamber had occurred.

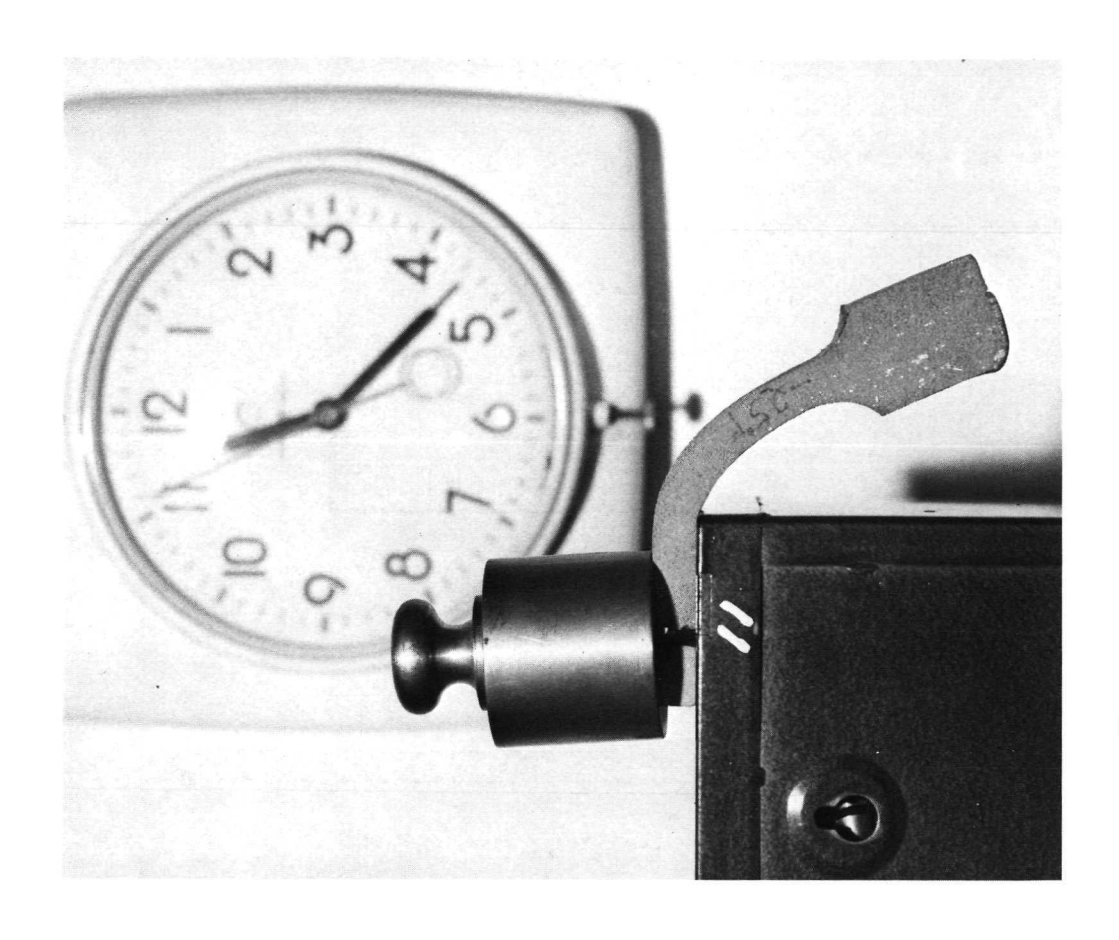
A later test at -29°C indicated no flaws but very slight buckling of the chamber. On conditioning the motor three days at -34.4°C, the propellant started to separate at the rim of the dished surface. At that temperature the modulus of the propellant is very high (7250 N/cm<sup>2</sup>) and its elongation is very low (about 4%). These tests were most gratifying. They indicate that significant margins in mechanical properties over a wider operating temperature range than necessary are available in the current decanol-modified propellants.

6. Motor Environment Tests. Propellant tailoring, described in part 3 of this section, had produced the low modulus propellant JPL 540 (Decanol/Trimodal) to avoid buckling thin flight-weight chambers or prevent propellant-to-insulation unbonding. The important question as to whether the modulus had been lowered too much was next investigated in the full 355-kg motor size in which the mass-to-shear surface ratio would approach that of a full scale Jupiter orbiter flight motor. However, to aggravate conditions and establish that margins exist for the propellant normally used, an extremely soft "slump motor" propellant was tailored with an elongation of about 178%, a maximum tensile strength of only 21 N/cm<sup>2</sup>, and a secant modulus of 12 N/cm<sup>2</sup>.

Figure 15 indicates how very soft it is. The tensile specimen after 11 s had deformed through an angle of about 55° under the stress of its own weight. Difficulty is experienced in machining this particular propellant because of its extreme softness.

The 355-kg motor using that very soft propellant was stored nozzle end down for 109 days at 22°C. Measurements at 8 preselected positions at the nozzle end indicated the maximum displacement was 0.6 cm. After 300 additional days in its normal storage position, nozzle end up, the maximum displacement was 0.3 cm. Finally, after an additional 30 days in the horizontal position, the greatest movement was 0.4 cm. When the motor was returned to the nozzle end up position, all of the points measured returned to within 0.21 cm of their original positions within one day.

For the vibration environment tests, JPL's Systems Division supplied a type-approval vibration program based on a representative launch vehicle environment (see Figure 16). An automatic sine programmer was employed to provide test continuity from 5 to 1500 Hz. The sweep rate was a very



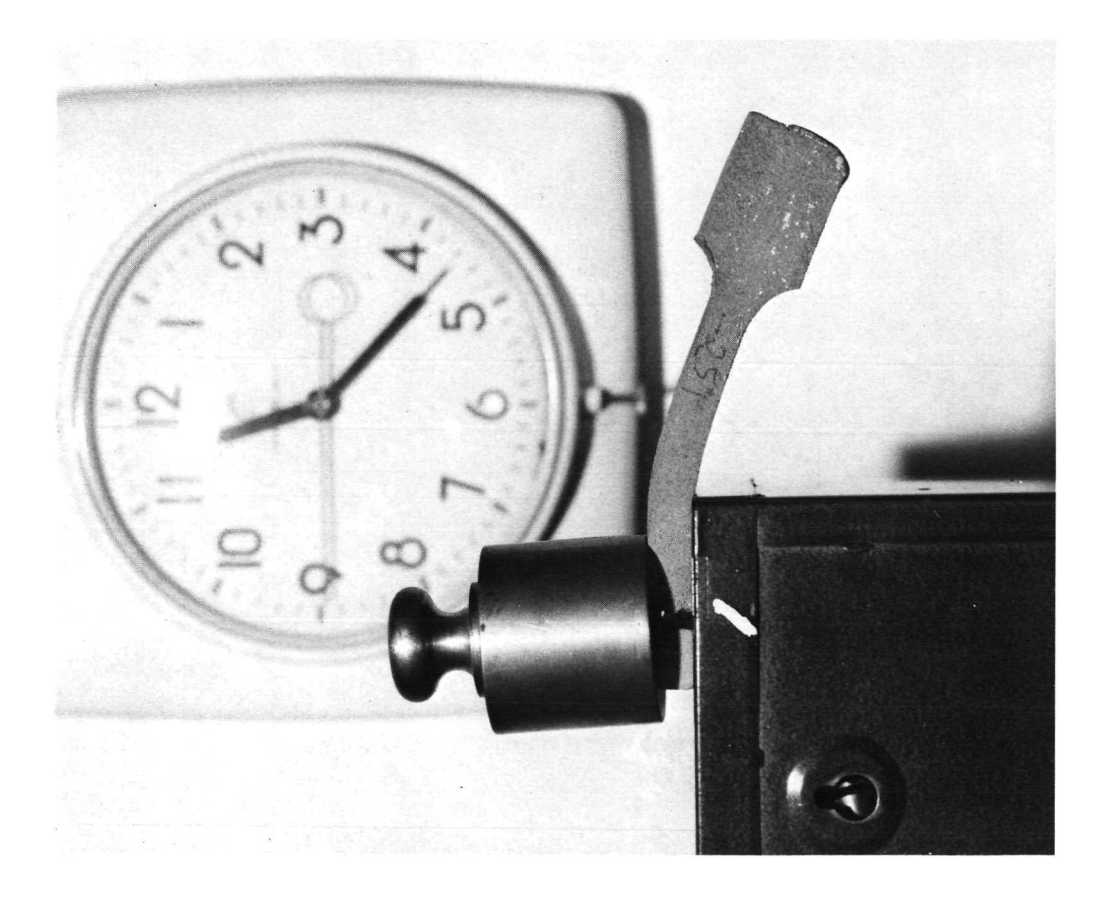


Figure 15. Slump motor propellant

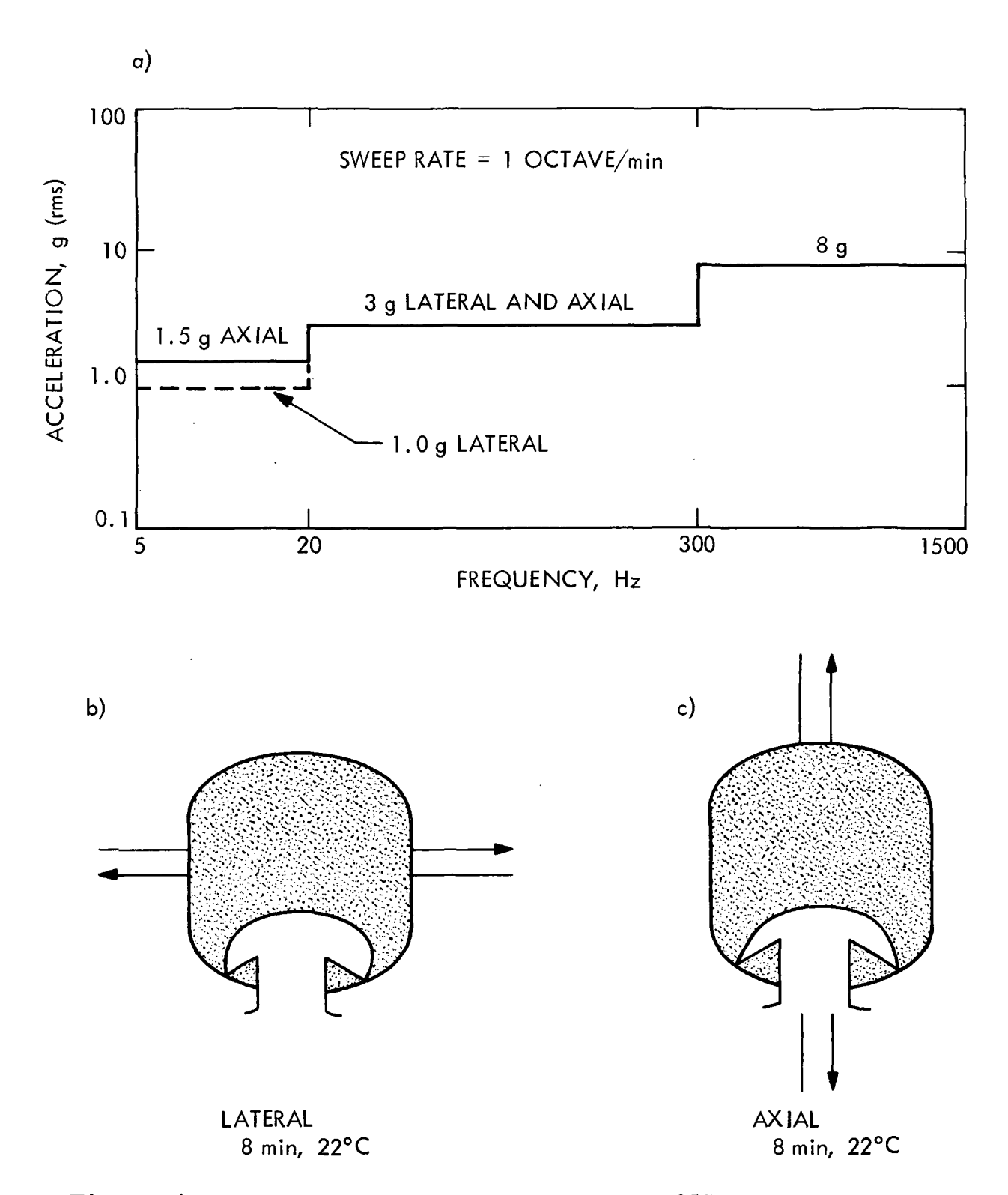


Figure 16. Launch simulation vibration tests on 355 kg slump motor

conservative 1 octave per minute so that each test took about 8 min. With the 355-kg slump motor mounted in the launch attitude position, nozzle down, vibration tests were made in the lateral direction, then in the axial direction. In the lateral direction, the maximum programmed input was 1 g from 5 to 20 Hz, 3 g from 20 to 300 Hz, and 8 g from 300 to 1500 Hz. The axial test inputs were the same except the level was 1.5 g from 5 to 20 Hz. Figure 17 shows the motor on the vibrator before its axial vibration test. The cylindrical shell around the motor supports it at the upper or forward attachment skirt, its normal spacecraft mounting ring.

All vibration levels are conservative, approximately 50% higher than the current TOPS or Viking type-approval system test levels, and thus provide margin for design and structural amplification uncertainties. The maximum induced acceleration, on the propellant surface, was in excess of 20 g. The maximum permanent propellant surface displacements from the vibration tests were only 0.79 cm, well within that considered acceptable. These test results were most gratifying in view of the extreme softness of the slump motor propellant used.

It is tentatively concluded that there are no significant slump or vibration problems at ambient temperature and the range of mechanical properties over which case-bonded end-burning motors can be designed is relatively wide and a very practical range.

## B. Chamber Insulation

The insulation early in the program was that used in the Syncom and ATS programs, Gen-Gard-V-52 as supplied by the General Tire and Rubber Co. of Akron, Ohio. It is a butadiene-acrylonitrile rubber containing silica and asbestos fillers and supplied as sheets of controlled thickness (0.20 cm). Later a lower density and more effective insulator, Gen-Gard 4030 supplied

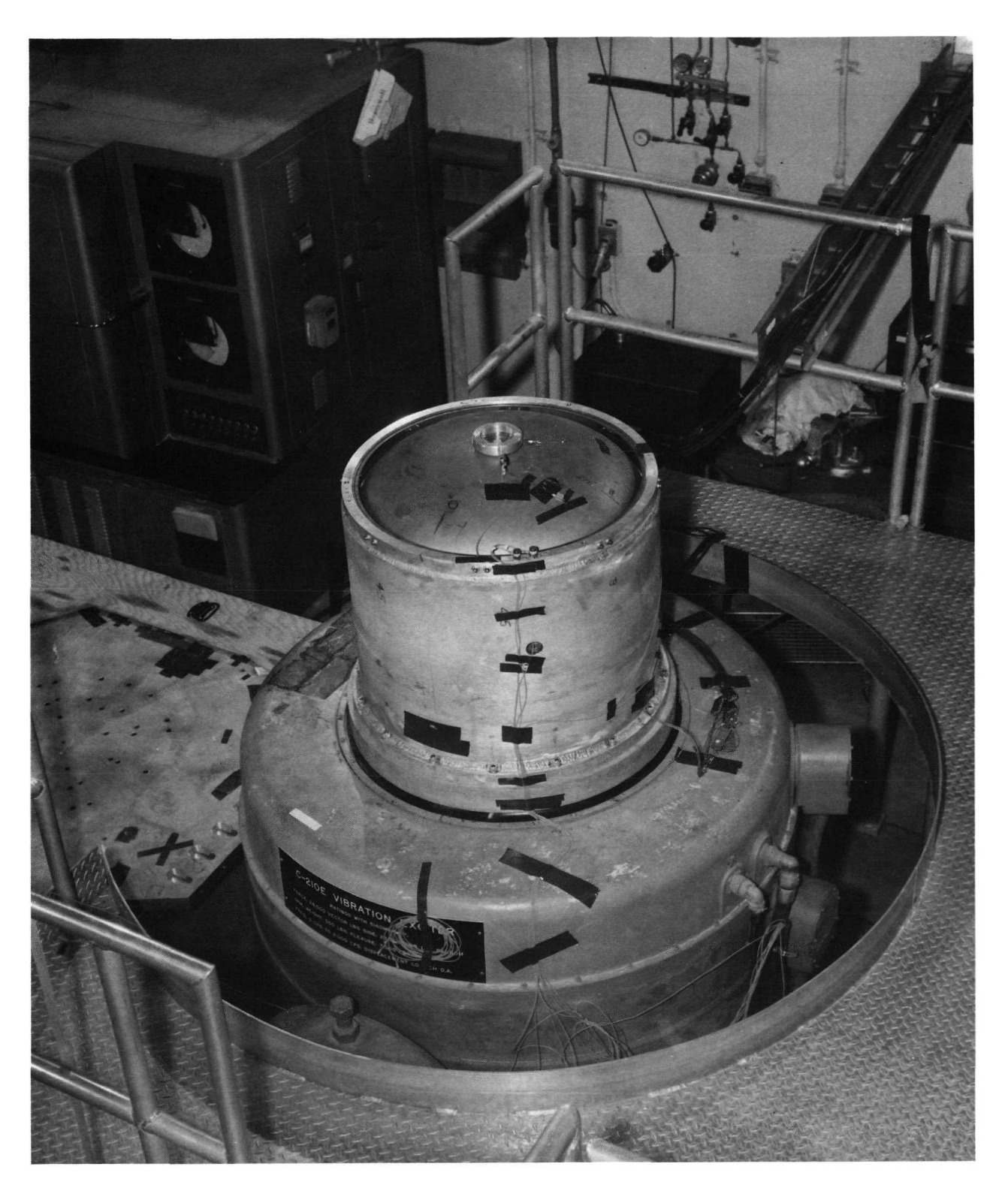


Figure 17. Slump motor before axial vibration test

by the same company, was adopted. It is an ethylene propylene terpolymer-based rubber (EPR) with silica and asbestos fillers.

The insulation is cut to pattern and is installed in layers by hand in a chamber which has previously been primed for rubber adhesion. After vacuum bagging to evacuate the gases between and around the layers, the insulation is consolidated and cured using internal chamber pressure on the insulation at 143°C.

Before casting the propellant into the chamber, the surface of the insulation is treated with a solution of toluene disocyanate in methylene chloride (25%:75% by weight) to promote bonding between the insulation and propellant during propellant cure. It is believed that the 5 min soak with the solution followed by overnight storage at 71°C in a forced convection oven to drive out the volatiles promotes softening and penetration of the insulation surface by the toluene diisocyanate. The latter is believed to react later with the hydroxyls in the propellant binder during cure to effect a chemical as well as mechanical bond at the interface. The excellent propellant insulation bond, even at high temperature, undoubtedly contributes markedly to the success of the case-bonded end-burning design. See section on Lower propellant burning rate and motor processing.

Recently an attempt was made to determine the combined erosion/char rate of the 4030 insulation as a function of the exposure time. As burning times have become longer it has been necessary to improve the prediction of required insulation thicknesses. The erosion/char thickness was evaluated experimentally by brushing away all residue of the charred insulation, measuring the thickness of the remaining virgin rubber as a function of station, or exposure time, then calculating the difference between the measured and

original thicknesses. See Figure 18 for plots of the thickness versus time as determined in the 355-kg demonstration firing D-1.

The results were not as reproducible as was desired because of occasional delaminations in the insulation layers and some flaking off of the char material during the firing, but an indication of the trend was found. Several curves of the form erosion/char thickness,  $T_{e/c}$ , =  $Ap^Bt^C$  were tried for fit. Where A = a constant; p = chamber pressure, N/cm<sup>2</sup>; t = time, s; B = pressure dependent exponent; C = time dependent exponent.

The pressure varied about 30% during the firing. It was assumed that the pressure exponent B was related to convective heat transfer and therefore had a value of 0.8. The two boundary curves were included to indicate the sensitivity to curve fitting. It is concluded that the erosion/char thickness variation with time is closer to the 0.5 power than to a direct proportionality. Although the equation is of limited accuracy, it was an aid in adjusting the thickness of insulation in the recent D-1A firing and will be used for the forthcoming D-2 firing.

## C. Low Acceleration-Rate Ignition

To prevent damage to delicate sensors on long flexible booms, or limit-cycling of the autopilot, the spacecraft acceleration rate, g-Dot, due to ignition thrust transients will be limited to about 0.3 g/s. Typical solid propellant motors, when ignited, build up thrust very rapidly (5 to 100 g/s), so that some scheme of gradual thrust buildup is needed.

Three approaches were considered initially:

(1) To mount a number of small, auxiliary solid propellant motors on the spacecraft to give precisely timed discrete increments or a gradual rise in thrust level.

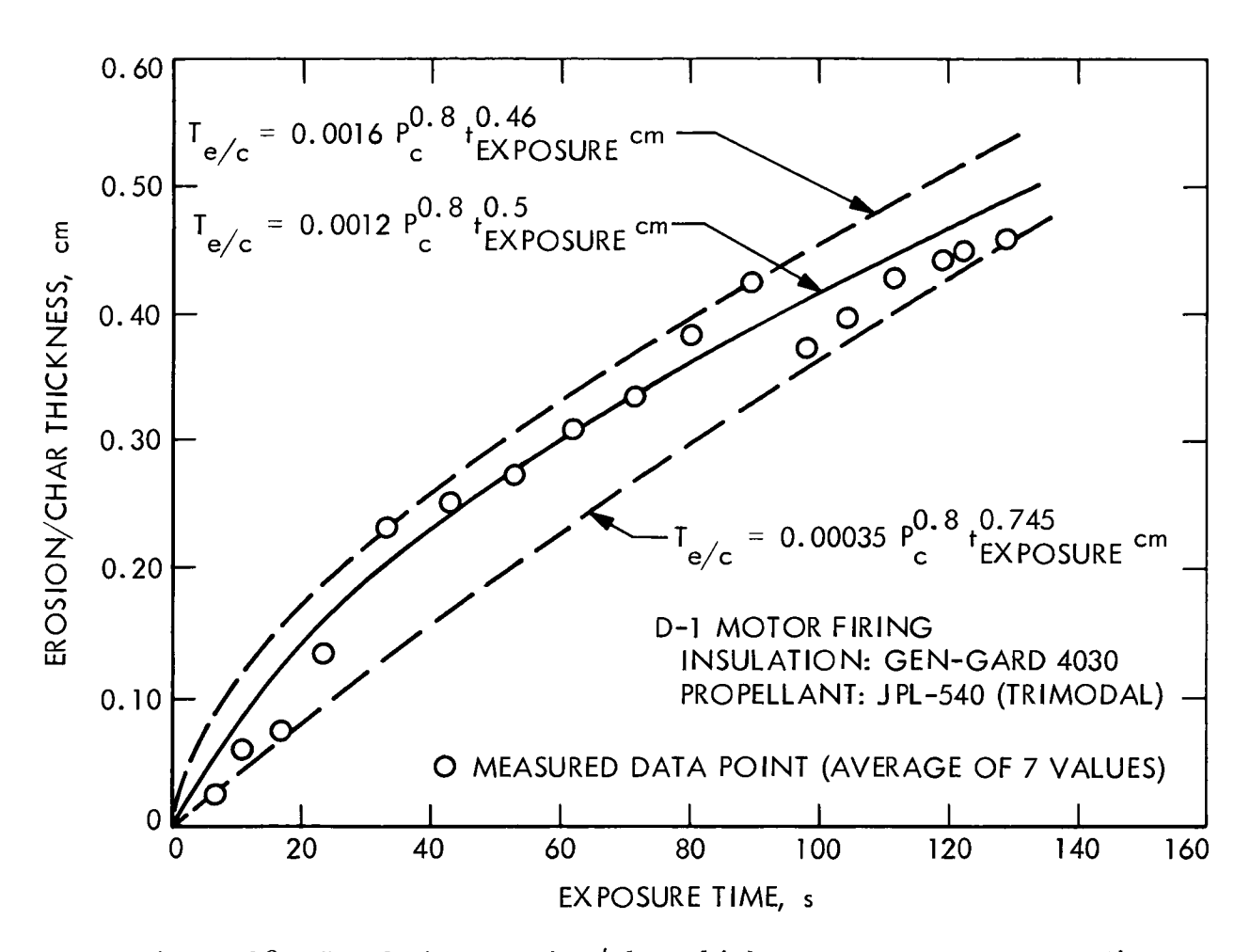


Figure 18. Insulation erosion/char thickness versus exposure time

- (2) To use a variable area nozzle throat, either ablative or pintle nozzle, along with an inhibited progressive burning surface to provide increasing thrust but at a chamber pressure maintained above the low pressure combustion instability limit.
- (3) To use a relatively long-duration controlled-flow igniter, having a regressive thrust program, in conjunction with a highly-inhibited rapidly-increasing burning surface in the main motor.

  This approach is an extension of the fluid control or mass excitation solid propellant motor concept advanced by the Propulsion Division of Lockheed Aircraft Co. of Redlands, California under NASA Contracts NAS7-444, NAS7-449, and NAS7-519.

Approach 3 was selected and an experimental program initiated to (1) demonstrate technical feasibility of the concept, and (2) generate design data and guidelines for later large-scale motor tests (Ref. 8). It is important to note that selection of the motor operating pressure influences greatly the ignition system design. When low chamber pressures are selected, then motor operation during a slow g-Dot ignition will be close to or below the L\* instability limit.

1. <u>Igniter Operation</u>. Operation of the igniter system can best be explained by reference to Figure 19, where motor D-2 is shown in cross section with the torus-shaped g-dot igniter mounted on the submerged portion of the nozzle. The igniter is actually a small solid-propellant motor that burns with sonic exhaust for about 1-1/2 s of its 2-1/2 s burning time. Its combustion gases pass radially outward from numerous nozzles, impinging on the dish-shaped propellant surface. Igniter pressure (absolute) decreases from about 241 N/cm<sup>2</sup> to about 124 N/cm<sup>2</sup>.

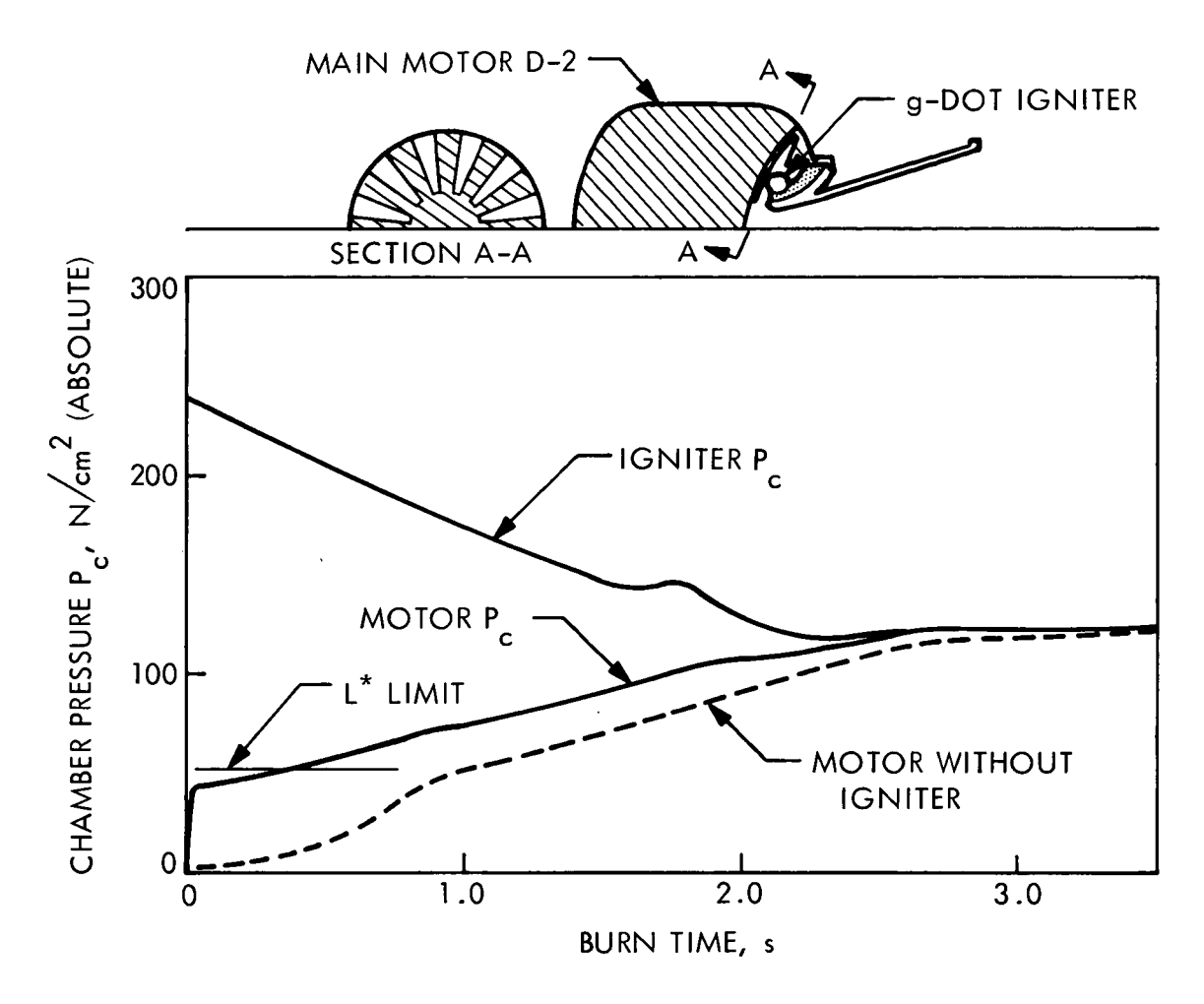


Figure 19. The g-Dot ignition concept

The main motor propellant burning surface is highly inhibited, as shown in section A-A of Figure 19, with an inhibiter pattern such as to produce highly progressive burning as the propellant surface regresses under the inhibitor. Thus, if the motor propellant could burn at a very low pressure by itself, its pressure-time curve would resemble the broken line in Figure 19 — with an initial pressure (absolute) of only 3.4 to 6.9 N/cm<sup>2</sup>.

In reality, because of the L\* combustion limit of about 44.8 N/cm<sup>2</sup> absolute, the motor would not burn by itself below that pressure. However, when hot exhaust gases from the independent controlled-flow igniter are injected into the main motor, the mass addition raises the motor pressure to about 34.5 to 37.9 N/cm<sup>2</sup> and burning of the main charge is sustained below the motor L\* limit by heat transfer and mass addition. The resultant low pressure and thrust level permit the spacecraft to meet its 0.3-g initial acceleration requirement.

The main propellant burning surface, and consequently chamber pressure, increases with time in a controlled manner until the motor is able to sustain combustion without mass addition from the igniter. The small, thin, inhibiter strips are partially, or completely, consumed before being ejected out of the nozzle.

It is believed that burning is sustained below the L\* combustion limit because of the decoupling effect of mass addition from the independent controlled-flow igniter on the combustion instability that occurs near the L\* extinction pressure. Thus, the combustion instability that promotes extinction of the burning is desensitized and suppressed by mass addition that is not a part of, nor influenced by, the main motor oscillations. Sonic flow in the igniter nozzles, of course, prevents any influence on the igniter pressure

by pressure fluctuations, i.e., oscillations, in the main motor. Reference 9 discusses the indicated type of combustion instability in more detail.

Key points that resulted from the small motor experimental program and influenced the igniter design may be summarized from Strand's report (Ref. 8):

- (1) "Feasibility was demonstrated in that motors were ignited at pressures significantly below their low-pressure L\* extinction limit (i.e., by as much as 30 N/cm<sup>2</sup>) and brought up to design pressure in a controlled manner."
- (2) "A quasi-steady state mass balance expression, with an assumed c\* efficiency 90% of theoretical was a useful tool for predicting the initial equilibrium pressure conditions in the insulated main motor and, to a lesser extent, for predicting the approximate main motor pressure program."
- bility that was sensitive to the motor characteristic length, L\*, and the igniter and main motor propellant mass flow rate ratio, mig/mmotor. Increasing the mass flow rate ratio depressed the motor L\* extinction pressure and reduced the amplitudes of the pressure oscillations, but the instability persisted at the L\* and motor pressure conditions investigated up to the highest mig mmotor tested. As predicted from present L\* instability theories, lowering the motor L\* increased the exponential growth rate constant for the amplitude of oscillations, producing stronger pressure oscillations and chuffing. It was concluded that the burning time in the low pressure instability region should be kept to a minimum, cutting down on the time for growth of the oscillation amplitudes."

2. <u>Some Practical Considerations</u>. Concern about potentially unacceptable spacecraft acceleration rates from these instability oscillations prompted a recent series of computer runs in which the effect of the oscillations on the spacecraft attitude controls was simulated using the Thermoelectric Outer-Planet Spacecraft model, modified to include the retropropulsion for a Jupiter orbiter mission. It was concluded that, for both rigid and flexible body dynamics, the oscillations arising from the use of the g-dot igniter and other low-amplitude bumps and spikes that may occur in the thrust profile had no apparent effect on the attitude control system.

In the same series of computer runs, the effect of initial acceleration during igniter initiation and the acceleration rate during igniter burning on the spacecraft controls was also evaluated. The following results were obtained:

Maximum initial acceleration, g	Acceleration rate during igniter burning, g/s	Effect on spacecraft controls
0.2	0.2	Acceptable
0.4	0.4	Acceptable
0.6	0.6	Limit cycling

Because tests were not all-encompassing in their scope, conservative values of 0.3-g maximum initial acceleration and 0.3-g/s acceleration rate were adopted as design criteria for the ignition system and motor thrust decay. When an actual spacecraft configuration is known, these design values must be reassessed.

The pressure-time relationships shown in Figure 19 represent idealized values. There was concern that, in reality, the normal ignition delay under vacuum conditions (typically 0.2 to 0.3 s in small motor g-Dot firings) might shift the mass flow rate ratio,  $m_{ig}/m_{motor}$ , to such a low value that a misfire would result.

Figure 20 shows the igniter pressure-time curve, and the results of the calculations for main motor pressure-time curves when motor ignition delays were assumed to be 0, 0.3, and 0.6 s. Results were obtained from an overall mass flow balance for the motor.

Fortunately the mass flow rate ratio was found to lie above the desired value of approximately one at the start of main motor burning for the given motor and igniter design conditions. Thus, it is believed that normal main motor ignition delays will cause no difficulties in the firing of the demonstration motor D-2. Accelerations and acceleration rates were also found to fall within the 0.3 allowable values.

3. g-Dot Igniter Design. Figure 21 shows the torus-shaped igniter implaced on the submerged nozzle in the motor cross-section; design features of the igniter are shown in Figure 22. Its outer diameter will be 28.7 cm and the small tube diameter will be about 5.33 cm, with a wall thickness ranging from 0.32 to 0.63 cm. The igniter case will be made of polycarbonate, a thermoplastic material, and will have 12 silica-phenolic nozzles equally spaced around the case and firing radially outward to promote flame spreading over the main propellant charge. Each nozzle will have a throat diameter of only 0.584 cm; therefore a propellant with only 2% aluminum has been selected to minimize changes in throat area and pressure from oxide deposition. The propellant weight is estimated at 1.07 kg; the inert weight, the same. A layer of 0.08 cm rubber insulation on the inside, and perhaps on the outside, helps protect the plastic case for its 2-1/2-s burning time. It has been designed with a safety factor of 2, based on limit loads.

The igniter case is unusual in that it uses a thermoplastic material.

There was concern that the main motor nozzle could become partially or completely obstructed (disastrously) if uncontrolled breakup of an empty,

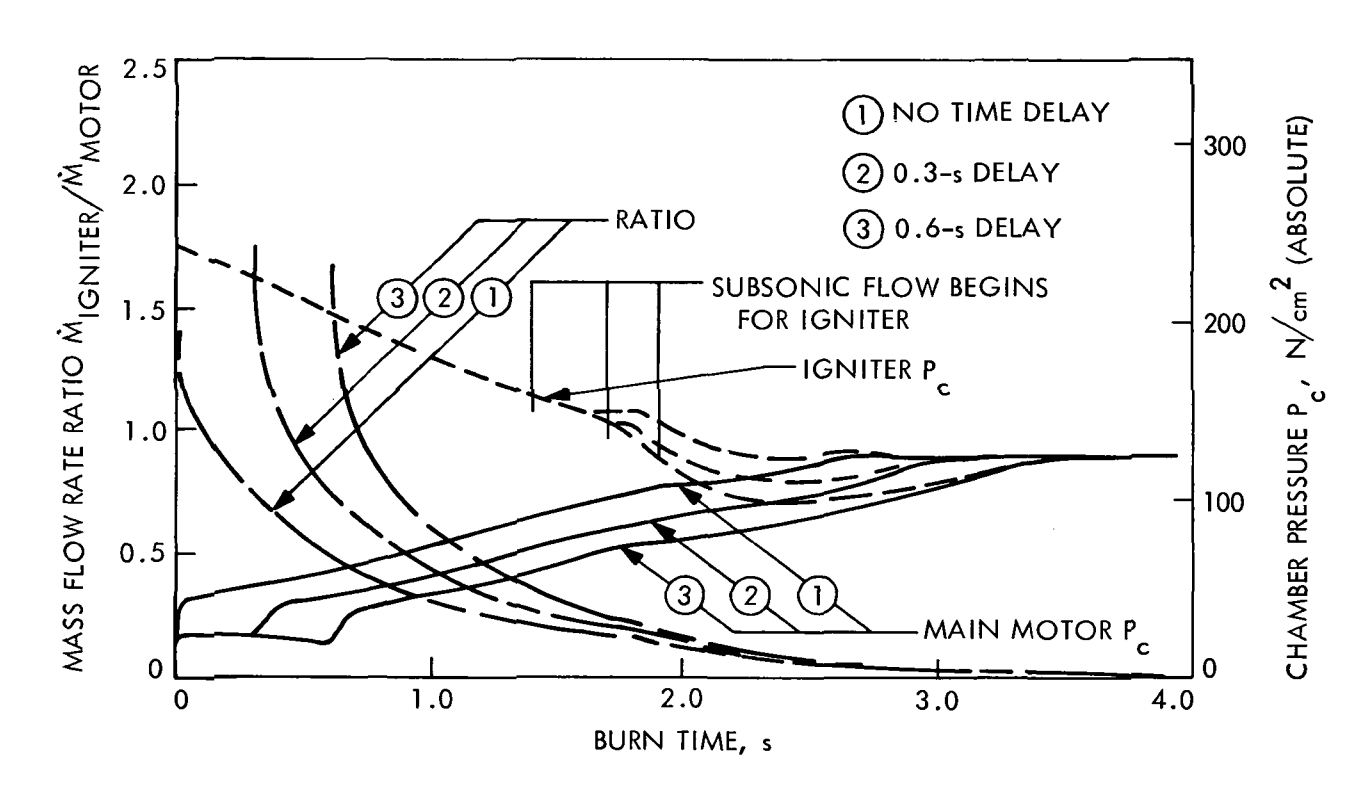


Figure 20. Mass flow rate ratio and chamber pressure versus burn time for main motor ignition delays of 0, 0.3, and 0.6 s

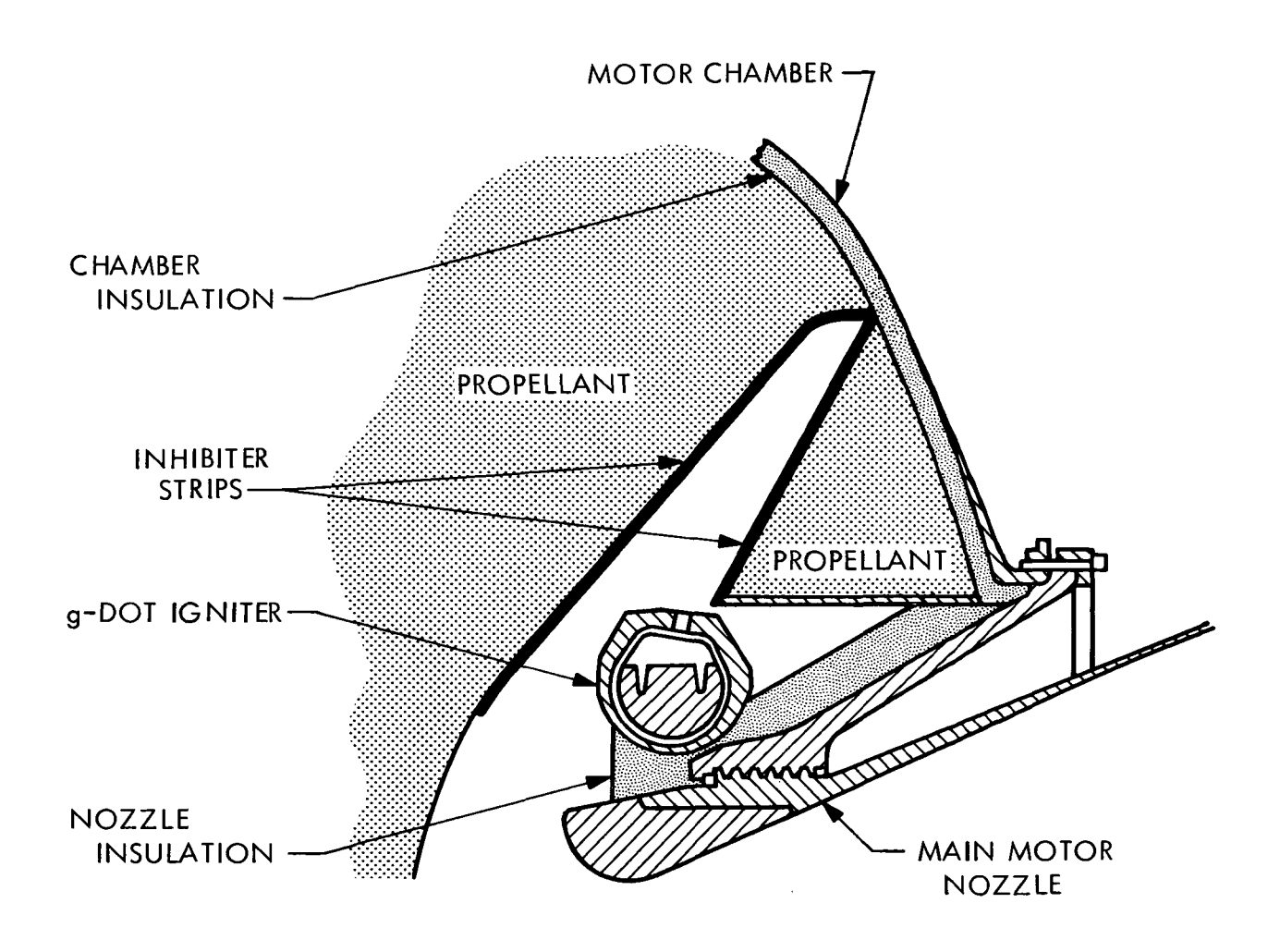


Figure 21. Igniter mounted in motor

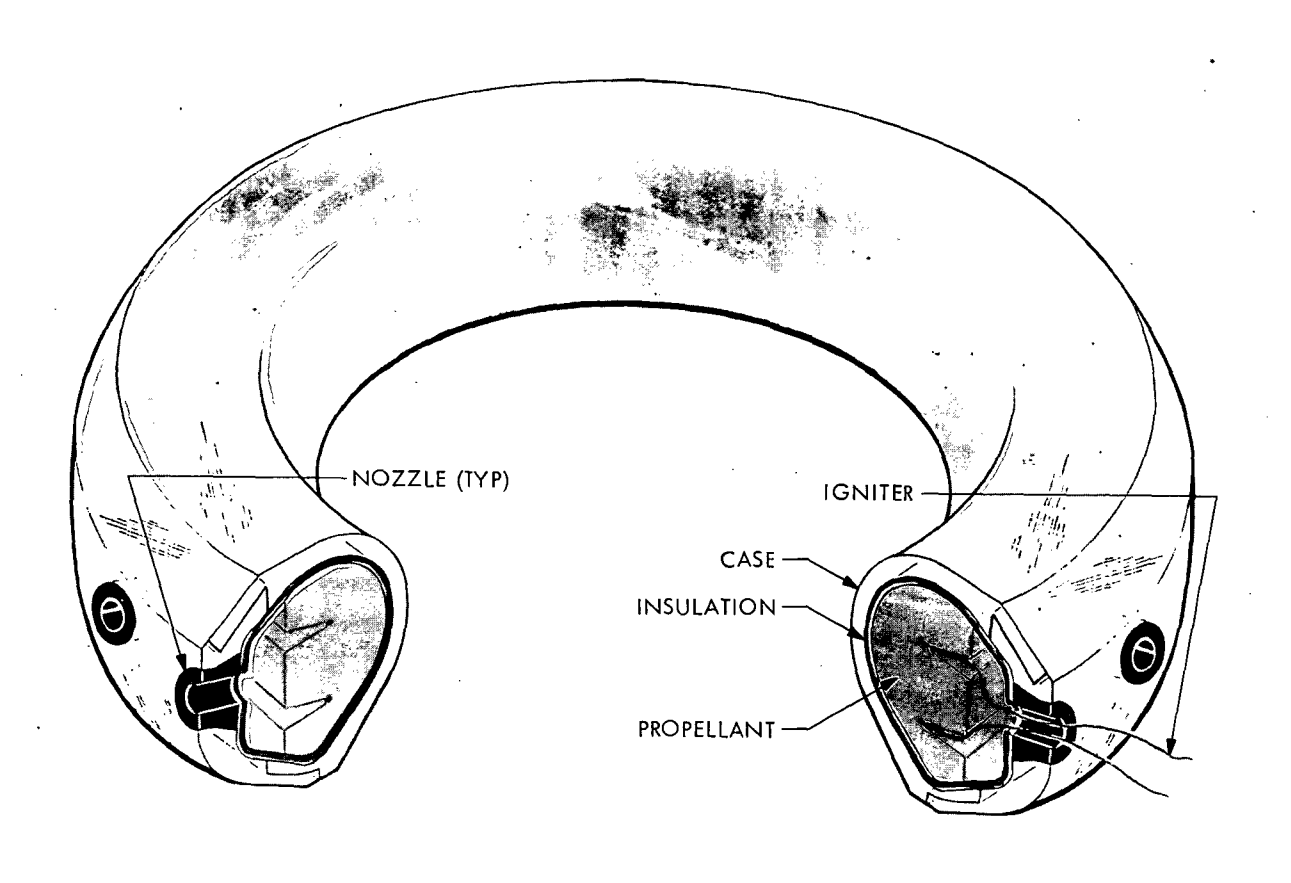


Figure 22. The g-dot igniter

hard or refractory, igniter case occurred during the long main motor burning. It is hoped the problem has been solved (1) by blocking the igniter into a cradle and cementing it to the nozzle phenolic insulation, and (2) through the use of a thermoplastic igniter case that will melt into a viscous mass around the nozzle and tend to wash away gradually into the stream of hot gases (c.f. Figure 21).

4. Processing and Igniter Testing. Although formation of the propellant charge in the torus case would appear to be difficult, practice tests have already revealed acceptable techniques. With a Teflon-coated split mandrel machined to form the finished propellant contour in place of the torus cover (Figure 22), propellant is vacuum-cast radially through the mandrel until a surplus fills the sprue. It is then cured for five days at 60°C, cooled, and the split mandrel removed. Before firing, the two sections of the torus are bonded together with an acrylic adhesive using a vacuum-bagging technique.

The polycarbonate case design has been qualified in a hydroburst test at 461 N/cm<sup>2</sup>; design maximum pressure was 276 N/cm<sup>2</sup>. Future testing will include a qualification static firing of the igniter alone in a vacuum tank, one or more firings in an ignition test motor that duplicates the ignition phase of the D-2 motor, a simulated altitude firing of the ignition test motor, and finally the firing of the demonstration motor D-2.

It is of interest to note that earlier in the program an improvised reinforced glass-plastic prototype of the igniter had been used to check out casting procedures, some nozzle design features, and the flame pattern at atmospheric pressure. Figure 23 looks down on the prototype igniter to show the exhaust pattern. The white circular grid indicates 5 cm radial intervals so that the flame extends well beyond the 35.5 cm radius of the main motor burning surface. A graphite nozzle insert was expelled late in

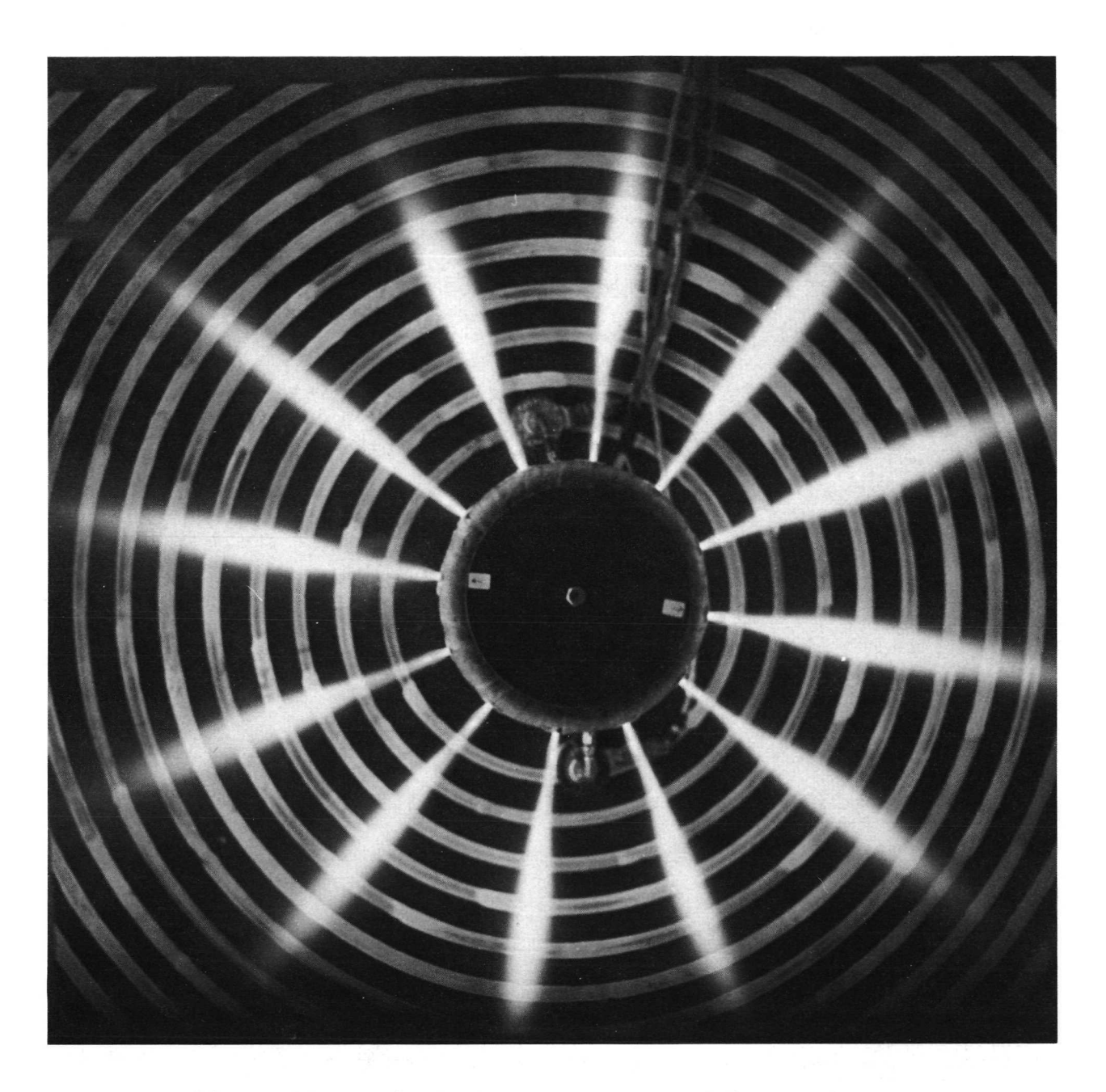


Figure 23. g-dot igniter prototype and flame pattern

the firing because of melting plastic; the silica phenolic insert remained intact and revealed a decrease in throat diameter of 0.017 cm.

## D. Nozzles for Long Burning Motors

Two approaches have been used to satisfy the requirements of lighter weight and long burning time nozzle capability: (1) use of improved or low density ablative nozzles, and (2) development of the all-carbon radiative nozzle.

In the May 28 firing of the 355-kg motor, a nozzle using a new low density (0.9 g/cm<sup>3</sup>) carbon-phenolic was fired. Earlier nozzles had been based on a carbon-phenolic in the structural section and silica-phenolic in the expansion cone. The weight of the low density nozzle was 15.33 kg compared to 16.8 kg for the ATS nozzle when the expansion ratio was 35 or an estimated 20.18 kg if the expansion ratios were the same, i.e., 75. Although some impingement from solid aluminum oxide particles in the exhaust gases eroded away part of the exit cone because of the off-optimum nozzle contour, the material is very promising for optimum contour and conical nozzles and would provide a substantial weight saving.

As burning time is increased for a given motor, however, one intuitively believes that a non-ablating radiative nozzle would, at some point, prove to be superior (lighter) than ablative nozzles. This assumes, of course, that the nozzle can be efficiently isolated, or insulated, from its thermally sensitive rocket motor chamber and that the severe thermal environment can be made acceptable to nearby spacecraft components. Efforts have concentrated on carbon structures because of their unique properties and because of significant strides recently by industry in fabricating the desired components.

1. <u>Nozzle Design</u>. Carbon filaments belong to a class of materials typically prepared from synthetic (e.g., rayon) fibers that, under controlled thermal decomposition in an inert atmosphere (i.e., pyrolysis), yield the desired carbon class of filaments. When advantageous, the carbon filaments may be graphitized to orient the carbon crystal structure to alter mechanical and thermal properties in preferred directions.

Carbon (graphite) filaments have been available for some time. However, the all-carbon composite class, i.e., the carbon (graphite) filaments or cloth in a carbon (graphite) matrix, is quite new, and there are several preparation processes under development by various manufacturers. The nozzle design described here capitalizes on the unusual properties of these carbon composites.

The mechanical strength and elongation of these materials increase with increasing temperature up to and above 3030 K. The mechanical and thermal properties are anisotropic; e.g., heat transfer across the fibers is significantly lower than that along the fibers. The tensile and compressive strengths are reasonably high, but the interlaminar shear, at present about  $1380 \text{ N/cm}^2$  is the weakest property and strongly influenced the design. These materials, as fabricated, are somewhat porous (density of about  $1.44 \text{ g/cm}^3$  versus 1.9 for high density bulk graphite), but the strong reinforcement fibers contribute markedly to toughness, an important factor during handling and ignition of the motor.

In the chemically reducing atmosphere typical of solid rocket combustion gases, these composites are relatively inert so nozzle erosion was expected to be low. Sublimation temperature reportedly is about 3922°K, well above the flame temperature of the propellant system used for the design.

The nozzle assembly (Figure 24) includes a laminated nozzle body of pyrolyzed graphite tape fabricated by the rosette pattern technique, a high-density graphite insert for the throat for maximum erosion resistance, and a laminated conical transition section of graphite tape oriented to minimize heat transfer. The transition, when mated to the chamber, supports the nozzle in a submerged position. Its gas seal at the chamber is a silicone O-ring; the seal at the threaded nozzle joint is a graphite gasket and ceramic cement. The thickness of most of the expansion cone is only 0.165 cm, the minimum that could be fabricated with confidence at the time the nozzle was produced.

In the design philosophy adopted, the extremely hot nozzle was retained by providing a long enough heat path along the conical transition section such that the heat-treated chamber would not be weakened unacceptably during the heating transient of the required burning time. Obviously, the transition section, with this design requirement, must be insulated on its lateral surface from propellant combustion gases at  $3161^{\circ}$ K temperature. A low-density  $(0.9-g/\text{cm}^3)$  ablative composite based on a phenolic-impregnated paper carbon serves as insulation.

Nozzle Fabrication. Success of the all-carbon nozzle work depended strongly on the knowledge and experience of industry, especially regarding material choice and nozzle fabrication procedures; design and feasibility testing were JPL's responsibility. Early development efforts were based on a filament-wound graphite nozzle body, but it was found that, during a late processing step (high-temperature graphitizing), significant cracks or delaminations developed or porosity proved to be unacceptably high in the pyrolyzed part. Subsequently, Reflective Laminates, a division of

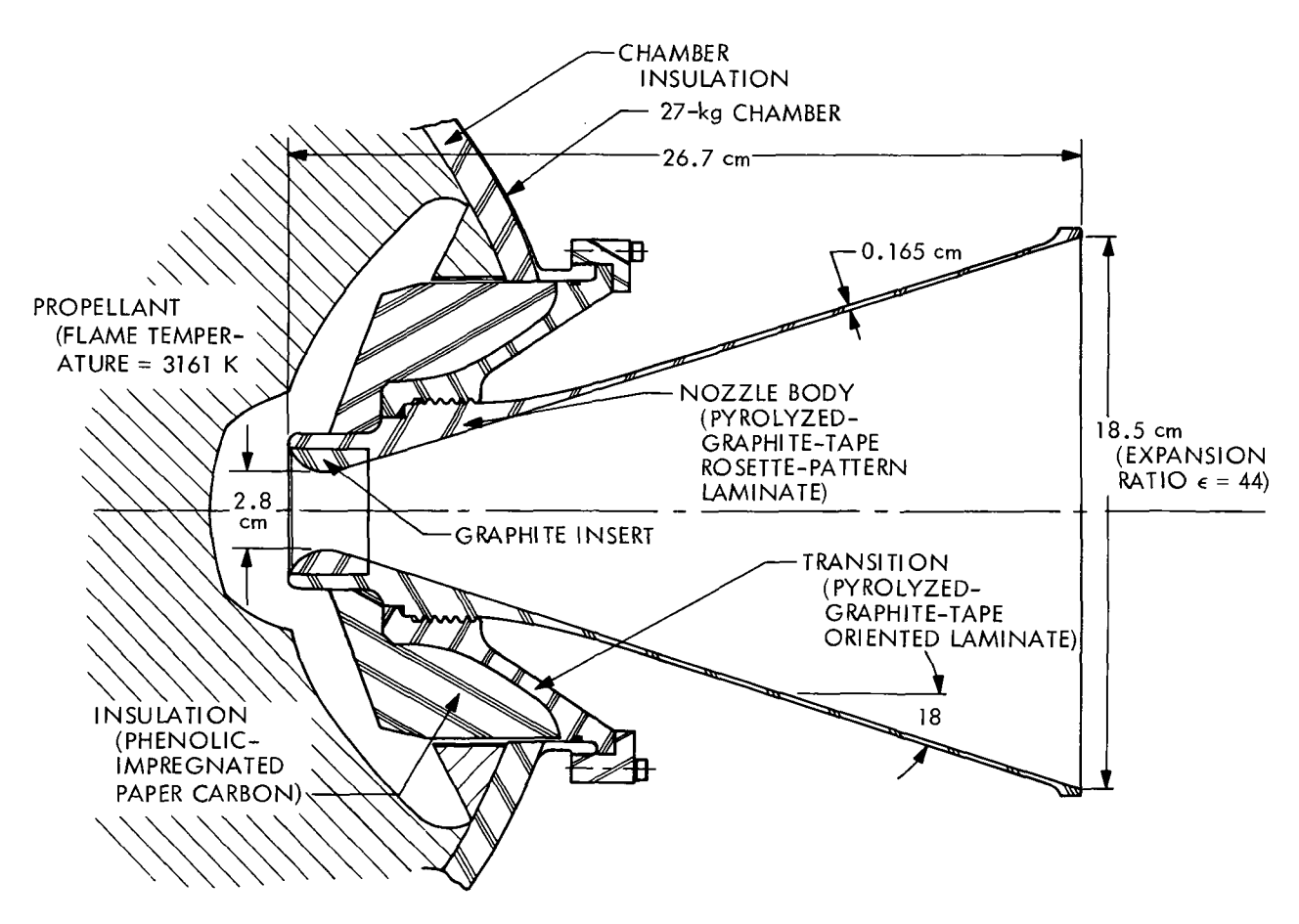


Figure 24. Configuration of all-carbon nozzle for feasibility testing

Fansteel, Inc., succeeded in producing satisfactory nozzle components by using graphite cloth in place of the filament-wound graphite.

Materials and procedures were specially designed for the fabrication of the carbon-to-carbon bonded structures. During processing, the interlaminar bond strengths are reduced, and the shrinkage stresses of the components increase. Therefore, procedures had to be tailored to process the components through these critical cycles without producing cracks or delaminations. The fabricator reports that the final part must be stress-relieved if interlaminar shear values in excess of 1380 N/cm<sup>2</sup> are to be produced.

Figure 25 illustrates the method used for producing the oriented laminated transition and the rosette-pattern laminated nozzle body. In essence, the procedure for producing these components consists of (1) making a large flat-plate laminated block and a thick-walled rosette-patterned laminated cone out of graphite cloth impregnated with phenolic resin, (2) rough-machining the two components from the block and cone, (3) subjecting these components to temperature pyrolyzing cycles, and (4) machining the components to their final configuration. The laminates are oriented in the block to increase the thermal resistance between the inside and outside diameters of the transition. The rosette pattern in the thick cone helps minimize shrinkage stresses and delaminations during the pyrolyzing steps.

The selection of a preimpregnated graphite cloth for making the block and thick-walled cone of Figure 2 was based on special requirements to produce uniform pyrolyzed components. The fabric must be selected for weave conditions and thermal stability of the fibers. The impregnating resin must have good char-forming characteristics with minimum shrinkage during polymerization. The resin solids content, volatiles, and flow must be

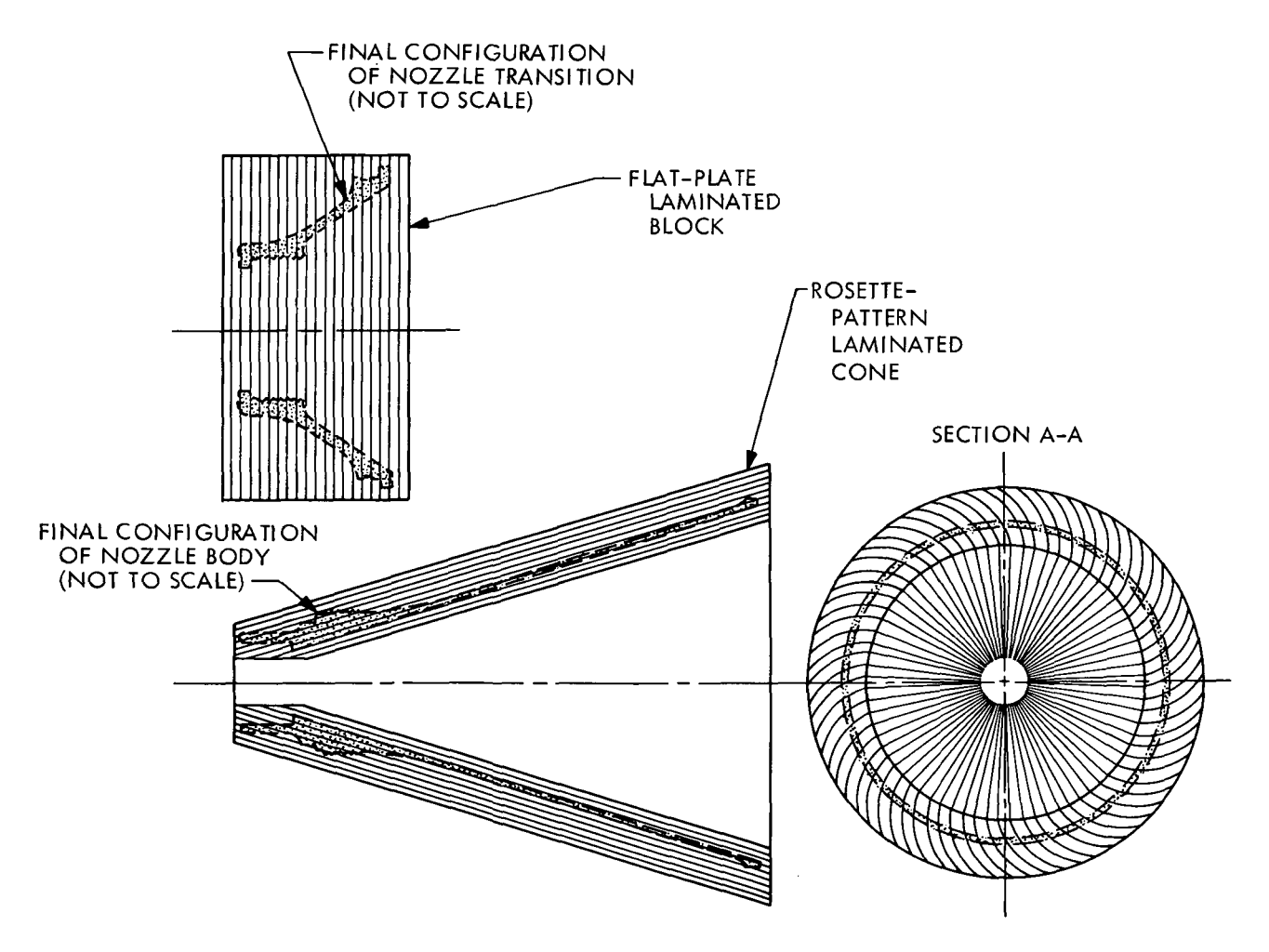


Figure 25. Layup step in nozzle transition and body fabrication

carefully controlled in the preimpregnated stage. The product meeting those requirements was a highly heat-treated graphite cloth impregnated with a phenolic resin with a solids content of 20 to 30%, and a maximum volatile content of 4%; the cured minimum acceptable density was  $1.4 \text{ g/cm}^3$ .

To obtain the required minimum density in the block and cone, several debulking cycles were performed at increasing pressures, but at temperatures low enough to prevent cure in the preimpregnated material. The block and cone were then cured at high pressure at 436°K and subsequently postcured at 506°K.

Following cure, the individual nozzle components were rough-machined, radiographed for cracks or delaminations, and subjected to a series of pyrolyzation cycles that carbonized the resin. Reimpregnation with a phenol-furfurol-based material after each cycle gradually raised the component density to that required. A final graphitization cycle was performed at 3030°K.

The components were again radiographically inspected for cracks or delaminations and were then machined to finished dimensions. Another radiographic inspection preceded the assembly of the components into the final configuration.

3. Static-Firing Test Results. The two finished nozzles were subjected to a total of three static-firing tests using flight-weight motors; the test conditions and results are summarized in Table IX. During the first test, conducted March 26, 1970, using nozzle SN-1, much of the nozzle body operated in a "white hot" mode for approximately 35 s of the 47-s burning time. After the firing, an inspection revealed no cracks or delaminations in the all-carbon transition and nozzle body sections and only small delaminations in the phenolic-impregnated paper carbon insulation. The nozzle was, in fact, judged to be in such good condition that it was subjected to another static firing test without refurbishment.

STATIC-FIRING TEST CONDITIONS AND RESULTS WITH ALL-CARBON NOZZLES TABLE IX.

	ALL-0	ALL-CARBON NOZZLES	LES	
ITEM	Test 1 (SN-1)	Test 2 (SN-1)	Test 3 (SN-2)	ABLATIVE NOZZLE
Propellant weight (kg)	26.65	25.42	26.65	27.57
Simulated altitude (km)	Sea level	Sea level	15.90	15.90
Motor burning time (s)	. 47	45	48	20
Nozzle expansion ratio	53.5	40.3	40.4	35
Maximum Chamber pressure (N/cm <sup>2</sup> )	196.6	146.3	157.4	172.5
Nozzle weight (kg)				
Initial	1.069	0.909	.0.987	1.981
Final	0.928	0.869	0.924	1.776
Throat diameter (cm)				
Initial	2.533	2.920	2.916	4.445
Final	2. 635	2. 998	2.954	4.465

The second firing resembled the first, except that the nozzle throat diameter was increased to test the motor and nozzle at pressure conditions closer to those desired for the ultimate flight application. The motor performed as expected. However, after an estimated 30 to 35 s of burning, a small rectangular hole (ultimately about 2.5 cm by 5 cm) developed in one side of the exit cone, at an expansion ratio  $\epsilon = 9$ , just downstream from the nozzle attachment ring plane. Since thrust was not being measured, the hole had no adverse affect on the motor performance. After sectioning the nozzle, the thickness at the edge of the hole was found to average 0.095 cm (compared with a fabricated thickness of 0.165 cm); no change in the internal diameter of the nozzle was noted. It was concluded that, since the nozzle was exposed to the air during the test, rapid oxidation on the outer surface of the cone resulted in the weak area and subsequent formation of the hole. It is believed that the nozzle would not have failed if the atmosphere had been inert or absent. The rest of the nozzle, especially the transition section, showed no abnormal effects after a cumulative 91 s of testing.

A third test, using nozzle SN-2, was made under simulated altitude conditions to test the high-expansion-ratio cone at full flow and to verify that the cone thickness, without oxygen exposure, would remain unchanged. Figure 26, a photograph taken about 30 s into the firing, shows the nozzle exhausting downward into the diffusor and illustrates the typical temperature gradient along the expansion cone. This nozzle was also found to be in excellent condition after testing, as shown in Figure 27. No cracks, delaminations, or changes in cone thickness from oxidation could be detected upon post-fire inspection. It is currently planned to refire this nozzle.

These all-carbon nozzles are about the same size as the flight nozzle used successfully on the JPL Syncom apogee kick motor (SR-12-1). Typical

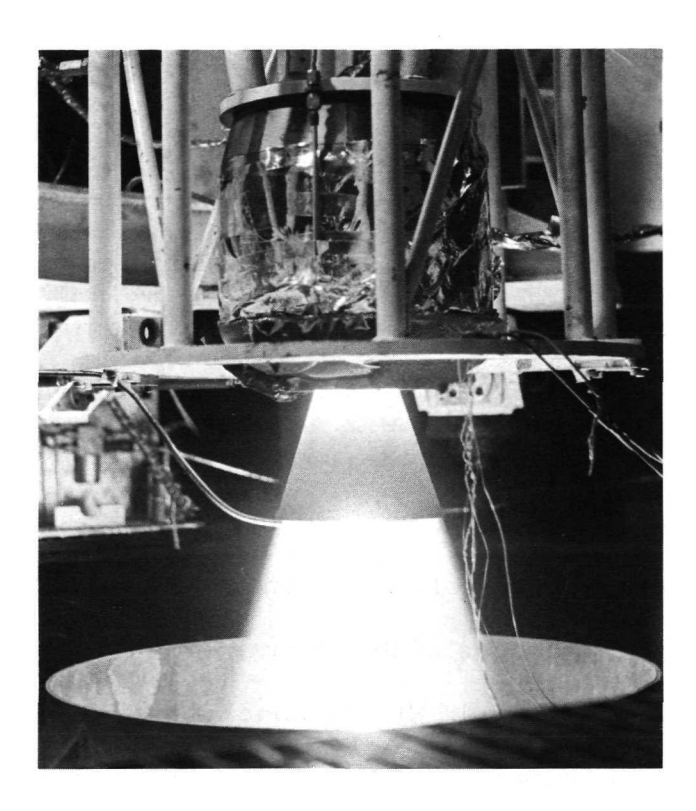


Figure 26. All-carbon nozzle during simulated altitude firing





Figure 27. All-carbon nozzle (a) before and (b) after simulated altitude firing

1964 test results of the Syncom nozzle are also presented in Table IX for comparison purposes. The Syncom motor used an ablative nozzle that was fabricated with a randomly oriented carbon-phenolic material. It was approximately 100% heavier than the all-carbon nozzles. It should also be noted that the Syncom nozzle could be used for only one motor firing of 20-s duration.

Figure 28 illustrates the nozzle surface temperature variation with time as measured by two infrared radiometers during the second SN-1 firing and the SN-2 firing at altitude. During the SN-1 nozzle test, the radiometers were focused at station 1, where  $\epsilon = 7$  (i.e., about 2.5 cm downstream from the nozzle-to-transition joint). During the SN-2 nozzle test, one radiometer was focused at station 2, where  $\epsilon = 27$  (i.e., 7.6 cm upstream of the nozzle exit). The maximum temperature measured at station 1 was about 1845°K; that at station 2 was about 1666°K. These values agree within about 55 to 83°K of the predicted temperatures at those stations — good agreement considering the limited data available on the thermal properties of these newly developed materials and the radiometer accuracies under the test conditions.

Conservative calculations were made to determine whether radiation losses would contribute significantly to a loss in specific impulse. They showed that (1) such losses, based on measured heat fluxes from the nozzle, did not exceed 0.6%, and (2) total nozzle heat losses did not exceed 1.2%, a typical value for small ablative flight-weight nozzles. A separate determination of the loss in specific impulse due to combustion gases flowing radially outward through the relatively porous walls of the nozzle cone revealed that such a loss was insignificant (<0.1%). Thus, the use of all-carbon radiating nozzles would not appear to have a deleterious effect on motor performance.

4. Thermal Analysis of Scaled-Up Nozzle. Ultimately, the 355-kg demonstration motor D-2, utilizing a scaled-up version of these all-carbon nozzles,

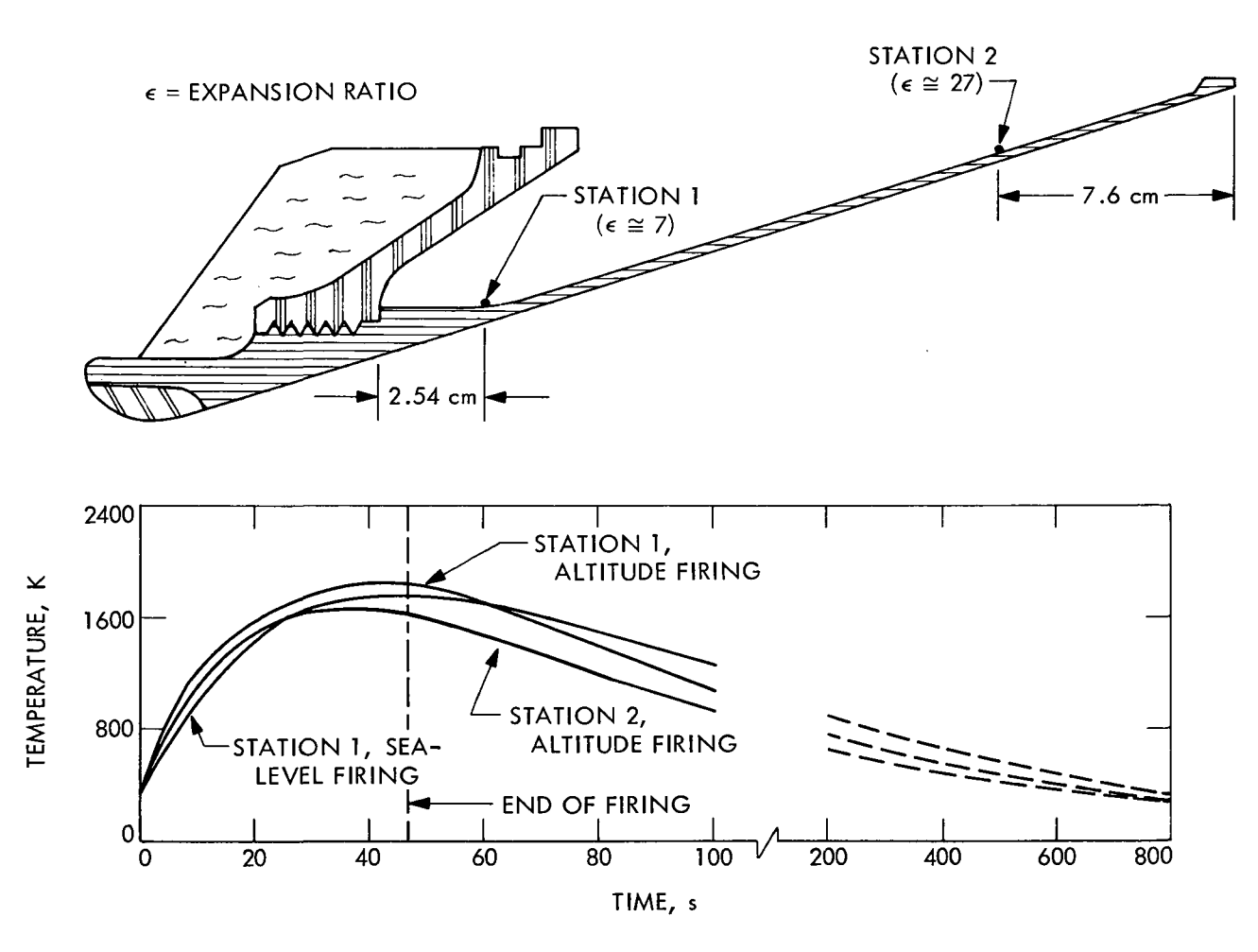


Figure 28. Measured nozzle surface temperatures during and after static firing of flight-weight motor

will be tested. In preparation for the firing of this motor with a 140- to 150-s burning time, a thermal analysis of a full-sized nozzle was made. Basically, the design used the same materials and concepts as those of the small-nozzle design. However, a sandwich-type heat shield [i.e., 1.3-cm-thick, low-density (0.08 g/cm³) carbon felt between aluminum plates, each 0.051-cm thick] was introduced to protect the aft end of the motor case. In addition, a 0.63-cm-thick layer of low-density carbon felt was incorporated as a thermal barrier between the transition and nozzle cone. The thermal model was set up and analyzed using the JPL CINDA computer program, which is capable of handling combined conduction, convection, and radiation for transient and steady-state conditions.

Figure 29 plots the predicted temperature versus time at five stations on the nozzle body and five stations on the conical transition member. The calculations indicate that, at the end of burning, the nozzle cone temperature will vary from 2390°K near its junction with the transition member to 1140°K near the nozzle exit. The transition member easily provides the pronounced temperature gradient needed to protect the chamber. The temperature of the chamber at the nozzle attachment point is expected to be only 375°K, an acceptable design value. The aluminum heat shield at node 184 should reach 547°K, well below its melting point. The temperature of the shielded case will rise an insignificant amount due to heat from the nozzle; e.g., node 150 should rise about 1 to 2°K.

Separate computer runs revealed that motor burning times up to 200 to 225 s are feasible with the indicated basic design for very small increases in insulation weight, provided the chamber pressures are kept low. It is of interest to note that the total nozzle, including insulation and heat shield, is estimated to weigh 9.8 kg. That weight can be compared with 15.3 kg for the lightweight ablative nozzle tested on the D-1A motor May 28, as mentioned

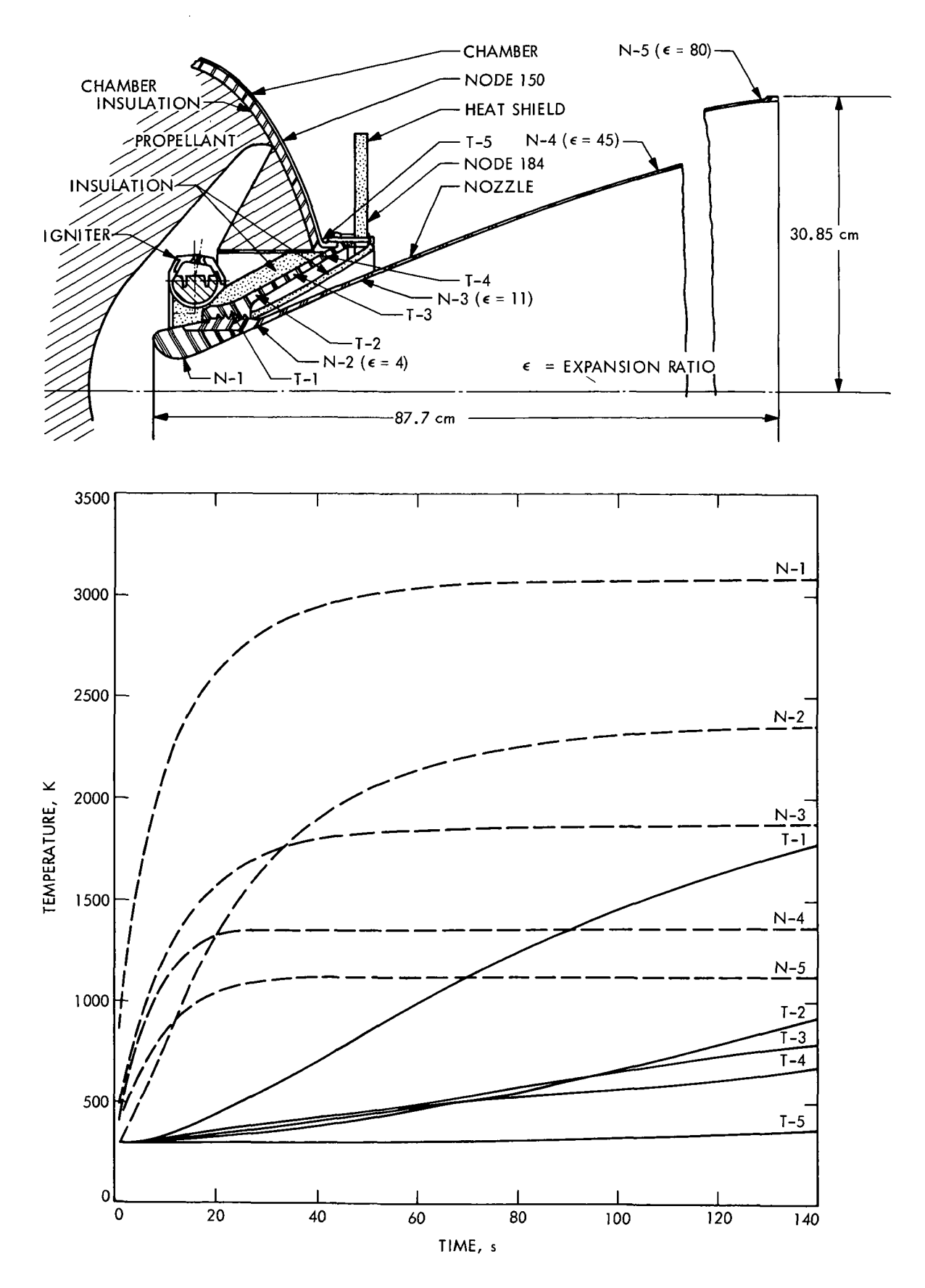


Figure 29. Predicted nozzle temperatures of 355 kg demonstration motor D-2

## V. DEMONSTRATION FIRINGS D-1 AND D-1A

Three static firings of the full-sized 355-kg demonstration motor have been made. Motor characteristics are shown in Table X and static firing results are given in Table XI. As mentioned earlier, motor T10 (demonstration D-0) was used to establish feasibility.

## A. Demonstration Firing D-1

Motor T12A was fired at simulated altitude to obtain vacuum I<sub>sp</sub> of the JPL 540 (Trimodal) Propellant, to demonstrate a 20-s longer burning time at higher pressure with the new Gen-Gard 4030 chamber insulation, and to obtain design data for the high-expansion ratio nozzle under full flow conditions.

The 25-kg motor P55 had shown about a 1.5% loss in c\* and  $I_{\rm sp}$  when using JPL 540 (Trimodal). Unfortunately there was a zero shift in the load cell during the firing of D-l so that the vacuum  $I_{\rm sp}$  appears suspiciously high. The c\*, however, appears consistent with reference radial-burning c\* data at higher pressure.

The lighter weight EPR insulation performed effectively in general though some delaminations were noted during postfire inspection. The maximum chamber temperature measured during the firing was only 65°C, well within the design temperature.

The ablative nozzle exhibited some aluminum oxide deposition on the aft 5 to 6 cm and a negligible amount of erosion in that region. The nozzle contour is off-optimum for the high expansion ratio in use. The throat, as noted in the table, eroded a little more than previously because of the higher pressure and longer burning time.

Strong evidence that there is no propellant cracking or charge separation in the case-bonded end-burner during the firing was given in the pressure-time record. This motor used the new low modulus propellant EB-27, containing

TABLE X. CHARACTERISTICS OF 355 kg DEMONSTRATION MOTORS

		)		
MOTOR	FLIGHT ATS	T10A	T12A	T9A
PURPOSE	Reference	Feasibility Firing	Vacuum Isp and design data	Vacuum Isp and component tests
BATCH NO. —		EB-8	BD-115	BD-125
CHARACTERISTIC				
Propellant Cure temperature °C Cure type Cure pressure (N/cm²) Maximum tensile strength (N/cm²)	JPL 540 60 Bulk 34 97	JPL 540 60 Zone 121 87	EB-27 60 Zone 121 46	JPL 541 60 Zone 121 54
Secant modulus, N/cm <sup>2</sup> Propellant weight (kg)	108 344. 7	12.7 68 353	26 355	37 355.1
Chamber (Titanium, 71 cm O. D. × 71.4 cm Long) Proof pressure (N/cm <sup>2</sup> ) Weight (kg)	207 11.07	155 11.07	155 11.07	190a 9.02b
Insulation Type Thickness (cm) Weight (kg)	Gen-Gard V-52 0.51 to 0.076 5.90	Gen-Gard V-52 1.0 to 0.20 16.96	Gen-Gard 4030 1.0 to 0.20 12.84	Gen-Gard 4030 1.25 to 0.25 16.78
Nozzle (Carbon Cloth-Phenolic) Expansion ratio Weight (kg)	35 16.78	11 10.43	63 30.40	75 15.33
Mass Fraction	0.906	Not Applicable	0.867	0.895
n				

<sup>a</sup>Proof tested at liquid nitrogen temperature <sup>b</sup>Chamber chemically milled to a wall thickness of 0.051 cm

STATIC FIRING RESULTS FOR 355 kg DEMONSTRATION MOTORS TABLE XI.

PARAMETER	FLIGHT ATS	D-0	D-1	D-1A
Motor	 	T-10A	T-12A	T-9A
Test date	Aug. 166	May '69	Apr. '70	May '71
Purpose	Reference	Feasibility firing	Vacuum I <sub>sp</sub> and design	Vacuum I <sub>sp</sub> and component tests
Motor temperature (°C)	15	15	15	15
Action time (s)	42.5	110	130	138
Mean effective pressure (N/cm <sup>2</sup> )	142	76.0	87.7	103.6
Maximum pressure (N/cm <sup>2</sup> )	180	94.0	107	120
Maximum thrust (N)	27,440	1 1	9474	8184
Propellant c* (m/s)	1515	1511	1509	1475
Average mass flow rate (kg/s)	8.11	3.21	2.73	2.57
Change in throat area (%)	1.5	0.3	2.2	3.2
Weight of $A1_2O_3$ slag (kg)	Trace	Trace	Trace	2.7
Vacuum specific impulse (N-s/kg)	2820	!!!	2932 <sup>a</sup>	2726
aTentative; unexpectedly high.				

decanol in the binder. Figure 30 shows the predicted and measured programs for motor D-1. Agreement is excellent even to slight increases in pressure at 33, 61, 92 and 117 s. At those points the insulation thickness in the chamber had been fabricated such as to decrease a discrete amount (the 0.2 cm thickness of one layer) and the propellant burning area and pressure, therefore, increased slightly. The discrepancy during the interval 15 to 25 s is explained by aluminum oxide deposition from the exhaust gases onto the nozzle throat; it washed away after 10 s as the nozzle heated. Nozzle coating often occurs with aluminized propellants. Hoop tension stress in the titanium chamber during the D-1 firing reached a value of 53,500 N/cm<sup>2</sup>; the chamber had been heat treated to an ultimate tensile strength of 103,500 N/cm<sup>2</sup>.

# B. Demonstration Firing D-1A

This most recent firing of the 355-kg motor at simulated altitude (15.9 km) had 5 objectives:

- (1) Static fire the motor with a mass fraction of 0.90 compared with 0.867 in the previous firing. It was actually 0.895 before the firing and 0.907 after.
- Obtain the vacuum specific impulse for the new low modulus propellant, JPL 541, (with 2-1/2% oxamide) and for a nozzle expansion rate of 75. The expected value was 2834 N-s/kg; the measured value was 2726 N-s/kg or 3.8% low. For the first time in a large-sized motor the measured c\* was also low, by 2%, and a large amount of aluminum oxide slag was produced in the motor (2.7 kg). Chemical analysis revealed that 45% of the slag was unburned aluminum. The latter, and the low I<sub>sp</sub>, are believed to result from the use of the oxamide, a coolant. As a potential solution to the low specific impulse result, consideration is

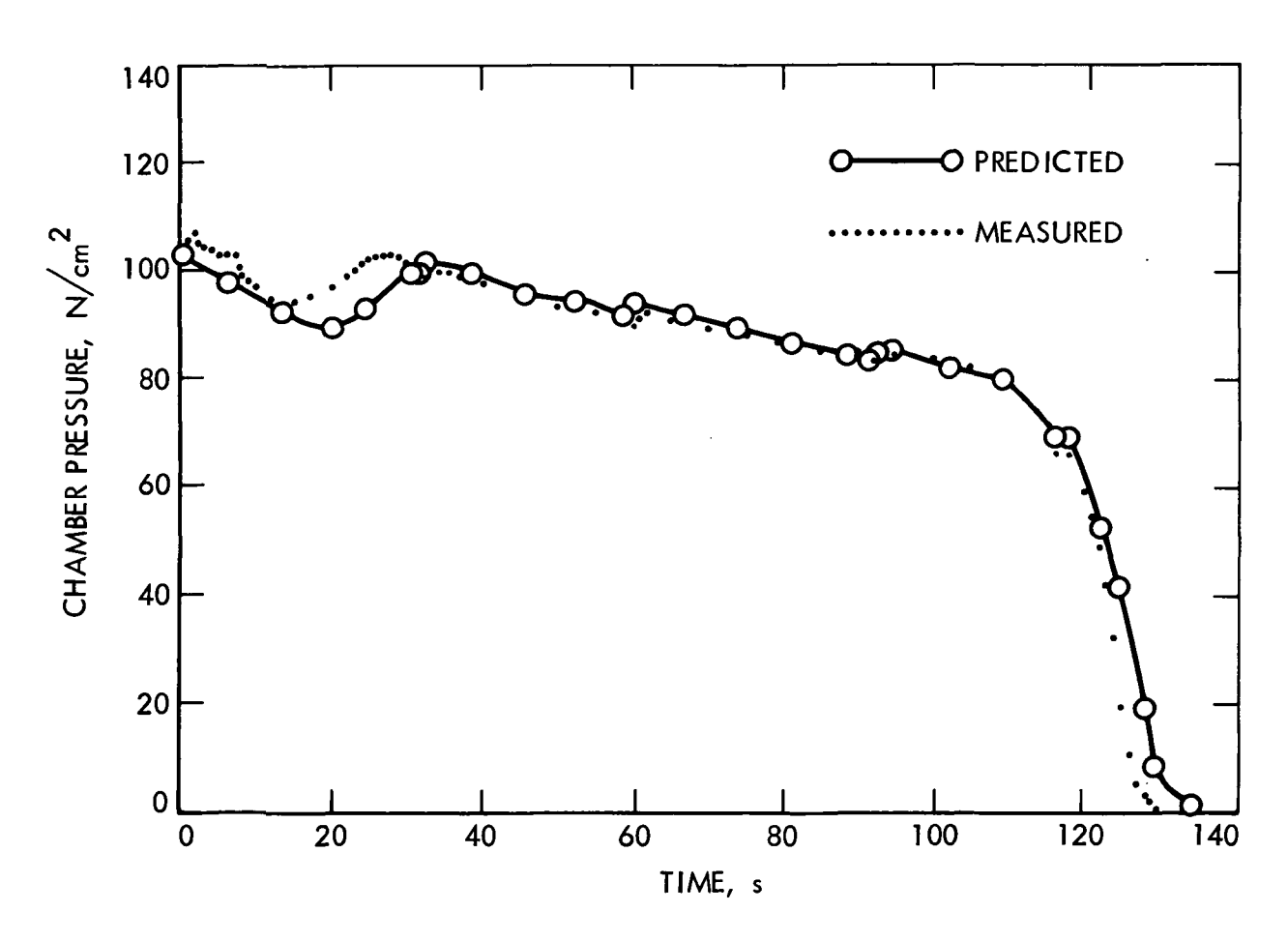


Figure 30. Predicted and measured pressure-time program for motor D-1

being given to a new urethane binder based on hydroxy-terminated polybutadiene with higher oxidizer concentration. It has inherently low burning rate and its high flame temperature should promote a high specific impulse efficiency.

- under very high chamber strain, i.e., higher pressure, 120 N/cm<sup>2</sup>, and thinner chamber wall, chemically-milled to 0.051-cm thickness. Under those conditions the hoop tension stress was 83,500 N/cm<sup>2</sup> or about 93% of the design stress for maximum pressure.

  The agreement between the predicted and measured pressure-time programs indicates no propellant cracking or pullaway at the associated high chamber strain values (c.f. Figure 31). Agreement between the two curves is excellent except for small discrepancies early in the firing that are undoubtedly due to slight deposition of aluminum oxide on the nozzle throat.
- (4) Refine the insulation equation for thickness-required versus exposure time. Significant delaminations between layers and even within layers were observed in the insulation after the firing and a hot spot the size of a small egg was found on the chamber.

  Producing good consolidation with this new EPR insulation appears to be a problem; indeed an error by the chamber insulating fabricator, who put about 25% too thick an insulator into the chamber, may have prevented a chamber burn-through.
- (5) Evaluate a new light-weight ablative nozzle weighing only 15.3 kg, i.e., 15.1 kg lighter than the ablative nozzle for the D-1 firing. The nozzle used a low density, 0.9 g/cm<sup>3</sup>, carbon phenolic tape wrapped to a thickness of 0.76 cm throughout the expansion cone.

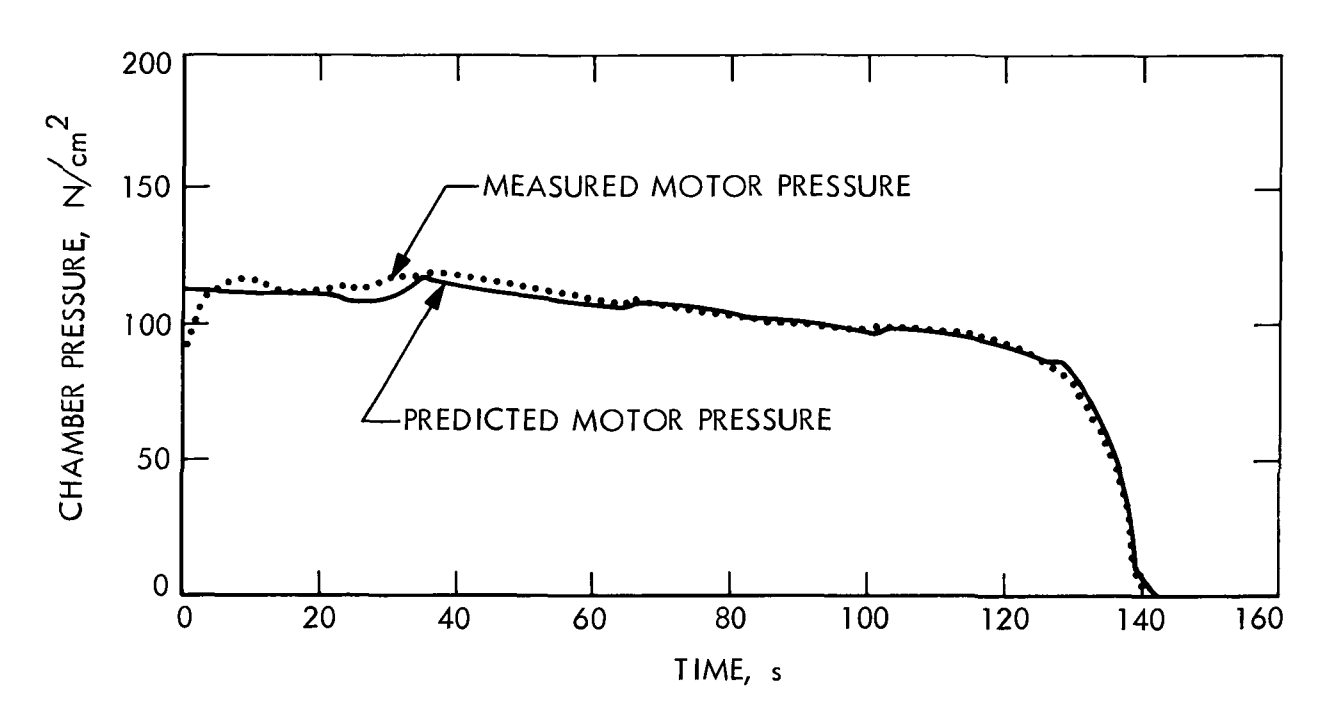


Figure 31. Predicted and measured pressure-time program for motor D-1A

A single layer of filament-wound fiberglass as a reinforcement for the cone was included also.

Its performance in general was satisfactory. However, the aft 7-1/2 cm of the cone eroded away; this is believed to be due to impinging high-velocity aluminum oxide particles. In the previous D-1 firing, light impingement with no erosion had occurred but the higher expansion ratio (to the same contour) in this firing resulted in severe aft-end erosion. A recontouring of the nozzle had been considered but it would have meant extensive computer calculations and a new expensive nozzle wrapping mandrel; thus, recontouring had been ruled out on a cost basis. The new low-density material does look very good for optimum contour and conical nozzles.

C. Comparison of Short and Long Duration Motor Performance.

Table XI indicates the mass fractions of the radial-burning short-duration ATS motor and the end-burning long-duration D-1A motor as tested. A better comparison results if the expansion ratio of the ATS nozzle is increased from 35 to 75 and if, at the same time, the new improved ablative material is used in the ATS nozzle. The ATS nozzle weight then becomes 20.18 kg.

In addition, stress analysis has shown that the existing attachment skirt for the motor is about 1.77 kg heavier than necessary for a Jupiter orbiter mission; thus, the two chamber weights in practice would become 9.30 kg and 7.26 kg for short and long duration motors respectively. The igniters used for each weighed 0.45 and 0.27 kg respectively.

Thus, the mass fractions, with "today's demonstrated state-of-the-art technology" in both motors, would be 0.906 for the short duration and 0.901 for the long duration motor of the same impulse. The long duration motor

value is, in reality, probably conservative; if better consolidation in the chamber insulation permitted the insulation weight to be that of demonstration motor D-1 then the mass fraction of the long duration motor would be 0.908. One may conclude that the performance of the two motors should be approximately the same.

### VI. CONCLUSIONS

At this stage in the long-burning motor program five conclusions can be drawn:

- (1) Controlled-flow igniters can be designed to sustain motor operation below the propellant L\* combustion limit as a mechanism for providing unusually low thrust and very gradual thrust transients.
- (2) Case-bonded end-burning motors using high-elongation, low-modulus propellant and high-pressure zone-curing processing provide predictable and reliable motor operation at room temperature, the only static test temperature evaluated.
- (3) All-carbon radiation nozzles appear very promising for increasing the mass fraction of long-burning motors which use submerged nozzles.
- (4) Despite the much longer burning times of the motors under development, their performance is essentially equal to shorter burning time motors of equal impulse.
- (5) The development effort has extended the technology of high performance solid propellant motors into a new regime for space applications; for a given thrust, burning times an order of magnitude longer than those of existing motors are potentially available.

#### REFERENCES

- 1. Robillard, C. L., and Cork, M. J., "Mission Constraints on Solid Propellant Motors for Unmanned Spacecraft," <u>Journal of Spacecraft</u> and Rockets, Vol. 6, pp. 745-748, June, 1969.
- 2. <u>JPL Outer Planet Orbiter Study</u>, conducted under auspices of office of Advanced Technical Studies, 1970 (Internal Communication).
- 3. Don, J. P., and Shafer, J. I., "Outer Planet Orbiter Propulsion,"

  <u>CPIA</u> Publication No. 196, Vol. I, 26th JANNAF Solid Propulsion Meeting held July 14-16, 1970 in Washington, D. C., (5/31/70).
- 4. Thiokol Chemical Corporation, Final Report on NASA Contract

  NAS7-784, Technology Development for High Performance, Low-Thrust

  Solid Propellant Rocket Motors, (In Preparation).
- 5. Holsapple, K. A., and Fourney, M. E., Stress Analysis of JPL End

  Burning De-Orbit Solid Propellant Motor, Task Report on Contract No.

  NAS 7-464, August 1970, Mathematical Sciences Northwest, Inc.,

  Seattle, Washington, 98105.
- 6. Marsh, H. E., Jr., and Udlock, D. E., "Formulating Propellants for Fully Case-Bonded End-Burning Motors," AIAA Paper No. 71-654 given at AIEE/SAE 7th Propulsion Joint Specialist Conference at Salt Lake City, June 14-18, 1971. NOTE: Paper available at AIAA New York Office until November 15, 1971; thereafter photoprint copies are available at photocopy prices from Technical Information Service, 750 3rd Ave., New York, New York 10017.
- 7. Smith, Robert C., Jr., "Effect of Ammonium Perchlorate Particle
  Size on Solid-Propellant Combustion Efficiency," Journal of Spacecraft
  and Rockets, Vol. 5, No. 11, pp. 1360-62, November 1968.

## REFERENCES (contd)

- 8. Strand, L. D., "Low-Acceleration Solid Propellant Rocket Ignition Study," Jet Propulsion Laboratory, Pasadena, California (In Preparation).
- 9. Beckstead, M. W., and Price, E. W., "Nonacoustic Combustor Instability," AIAA Journal, Vol. 5, No. 11, pp. 1989-1996, 1967.